

# Electric field induced half-metallicity in a two-dimensional ferromagnetic Janus VSSe bilayer

Khushboo Dange,<sup>\*</sup> Shivprasad S. Shastri,<sup>†</sup> and Alok Shukla<sup>‡</sup>

*Department of Physics, Indian Institute of Technology Bombay, Powai, Mumbai 400076, India*

Two-dimensional half-metals with intrinsic ferromagnetism hold great potential for applications in spintronics. In this study, we aim to expand the known space of such two-dimensional ferromagnetic (FM) half-metals by investigating a bilayer of Janus VSSe, an FM semiconductor. Its structural, electronic, and magnetic properties are examined using first-principles density functional theory (DFT) based approach, employing the DFT+ $U$  methodology, coupled with the PBE functional. The stability of the bilayer is examined using ab initio molecular dynamics simulations at finite temperatures up to 400 K. To ensure the stability further, the elastic constants of the system have also been investigated and we found that VSSe bilayer remains stable against structural deformation. The magnetic anisotropy calculations suggest that the VSSe bilayer manifests an easy plane of magnetization similar to its monolayer counterpart. At the DFT+ $U$  level of theory, the considered VSSe bilayer exhibits a tendency towards half-metallicity with a small band gap of 0.11 eV for the majority spin carriers, and of 0.60 eV for the minority ones. To induce a transition from a semiconductor to a half-metal, the bilayer is subjected to an external electric field of varying strengths normal to the plane. The lack of horizontal mirror symmetry in the bilayer allows bidirectional tuning of the band gap, with different values for the field in “upward” and “downward” directions. The band gaps for the two spin channels increase with the increasing upward applied electric field, while the opposite happens for the downward fields, with the majority carrier gap closing at  $\approx 0.16$  V/Å, making the material a spin gapless semiconductor. Further increase in the electric field renders the material half metallic at  $\approx 0.18$  V/Å. Given the fact that these values of the external electric field are achievable in the lab suggests that the FM Janus VSSe bilayer is a promising candidate for spintronic devices.

---

<sup>\*</sup> khushboodange@gmail.com

**Keywords:** Janus VSSe bilayer; density functional theory; electronic and magnetic properties; external electric field; band gap modulation; spintronics; spin gapless; half-metal

## I. INTRODUCTION

Spintronics is an emerging field that exploits the electron's spin in addition to its charge for advanced device applications. For such applications, the devices preferably require materials with 100 % spin polarization at the Fermi level, which is satisfied by the half-metallic ferromagnetic materials. These properties make them ideal for developing highly efficient spintronic components such as spin valves, magnetic tunnel junctions, and spin transistors [1]. Spintronics has the potential to revolutionize various technologies, including magnetic storage, data processing, and quantum computing, with reduced power consumption, high processing speed, and enhanced device functionality [2, 3]. Two-dimensional (2D) half-metallic ferromagnets are of great research interest in this field since they lead to miniaturization of devices in many important applications, in addition to the full spin polarization at the Fermi level offered by their bulk counterparts. Despite these promising applications, intrinsic 2D ferromagnetic (FM) half-metals are rare, with no practical realizations yet [4–9]. Consequently, research into 2D magnetic materials that can be engineered into FM half-metals in the presence of external perturbations is at the forefront of the field of spintronics.

The transition from a semiconductor to a metal, or half-metal, can be achieved through doping [7, 10], strain engineering [11], or by applying an external electric field [10, 12, 13]. Applying an external electric field as a perturbation is an effective method for tuning the band gap because it provides excellent control to the experimentalist, and does not require any changes to the material under investigation. The reduction of the band gap by applying an external electric field has been theoretically predicted in bilayer structures of hexagonal boron nitride [14], and transition-metal dichalcogenides [12], while for ZnO thin films it has been experimentally demonstrated [15]. Recent studies reported that 2D fully compensated ferrimagnetic materials with zero net magnetization can also show fully spin-polarized currents in the half-metallic states upon the application of an external electric field

---

<sup>†</sup> shastri1992@gmail.com

<sup>‡</sup> shukla@iitb.ac.in

[16, 17]. The transition from a semiconducting phase to a half-metal has been reported for the FM CrSBr monolayer and CrI<sub>3</sub>-CrGeTe<sub>3</sub> heterobilayer by applying external electric fields of strengths close to 0.4 V/Å [18], and 0.6 V/Å [19], respectively. However, the practical realization of such high electric field strengths is normally challenging, which drives the search for 2D magnetic materials where half-metallic behavior can be achieved at lower electric field strengths.

The family of 2D transition-metal dichalcogenides (TMDs) represents an emerging class of versatile materials, exhibiting a wide range of interesting electronic, optical, and magnetic properties [20]. First-principles calculations have predicted intrinsic long-range FM order in TMDs, when the underlying transition metal is V, Fe, or Mn [21–23]. The practical realization of long-range FM order in 2D magnets is challenging according to the Mermin-Wagner theorem, which states that magnetic ordering gets suppressed over long ranges when reduced to lower dimensions at any finite temperature [24]. Despite this, several atomically thin 2D van der Waal (vdW) magnets have been successfully synthesized, exhibiting long-range FM order [25–27]. This is due to the strong magnetic anisotropy in 2D magnetic materials, which provides thermal stability thus sustaining long-range magnetic order. Bonilla *et al.* [28] provided the first experimental evidence of intrinsic long-range FM order in a VSe<sub>2</sub> monolayer, marking it as the first 2D TMD to exhibit room-temperature ferromagnetism. The presence of this long range FM order makes the VSe<sub>2</sub> monolayer a promising candidate for spintronic devices as also suggested by theoretical studies [22]. Similarly, based on first-principles calculations, the VS<sub>2</sub> monolayer has been proposed for spintronic applications due to its predicted long-range FM order [21, 22].

Janus TMDs which are a new class of materials with broken horizontal mirror symmetry due to different chalcogen atoms on each side exhibit spontaneous polarization. This facilitates enhanced band gap tunability and Rashba spin splitting both of which are beneficial for spintronic and other applications [29–31]. The successful synthesis of 2D non-magnetic Janus MoSSe on the SiO<sub>2</sub>/Si substrate [32] has sparked an upsurge in research interest in the realm of 2D Janus materials, including vanadium-based Janus monolayers [31, 33, 34]. Janus VSSe monolayer is one such semiconductor, predicted to be stable in both the 2H and 1T phases, with the 2H phase and corresponding FM state being energetically more stable [31, 34]. Its dynamical stability has been reported in the literature by the absence of imaginary phonon frequencies [31, 34], while ab initio molecular dynamics calculations have

shown its thermal stability up to 500 K [35]. Due to broken time-reversal, inversion, and mirror symmetries, the FM Janus VSSe monolayer has strong response to external stimuli [31], thereby allowing easy tunability. As FM half-metals are superior for application in spintronics, FM semiconductor to FM half-metal transition of the 2D Janus VSSe will be particularly advantageous. This transition can be induced by an external electric field if the structure consists of a bilayer of magnetic atoms and the energy bands near the Fermi level correspond to the same spin channel, with different layer characteristics [18]. Therefore, in this work, from the perspective of applications in spintronics, we explore a bilayer of 2D Janus VSSe composed of different interfacial chalcogen layers, thereby retaining the broken symmetries of the monolayer. The properties of 2D Janus VSSe bilayer have not been studied in detail in the literature. For the purpose of benchmarking, we initiate our investigation by computing some intrinsic properties of the FM Janus VSSe monolayer, and compare them with the existing literature. Next, we simulate the bilayer formation by exploring three different stacking arrangements of the monolayers, and find that the most stable arrangement also exhibits FM order. Following this, we studied its structural, mechanical, electronic, and magnetic properties using first-principles density functional theory. The obtained band gap is lower compared to that of the monolayer for both the majority and minority spin carriers. We have explored the bidirectional tuning of the band gap by changing the magnitude and the direction of the perpendicular external electric field. We find that the external field in the “upward” direction increases the band gap, while, reversing the field has the opposite effect. In the latter case, at the applied field of  $\approx 0.18 \text{ V/\AA}$ , the gap closes for the majority spin carriers and a significant gap persists for the minority ones, resulting in a half-metal. The remainder of this paper is organized as follows. The next section deals with the discussion of the employed computational methods. Section III is dedicated to the presentation and discussion of our findings which are summarized and concluded in the last section.

## II. COMPUTATIONAL METHODOLOGY

Given the fact that the considered material is magnetic in nature, all the calculations were spin-polarized, and performed using the Vienna Ab initio Simulation Package (VASP) [36, 37] within the framework of the state-of-the-art density functional theory (DFT) [38, 39]. The kinetic energy cutoff has been set to 600 eV for the expansion of the Bloch wave func-

tions, using a plane wave basis set. The valence electronic configurations of V, S, and Se atoms are  $3d^34s^2$ ,  $3s^23p^4$ , and  $4s^24p^4$ , respectively, within the projector augmented wave (PAW) approach [40, 41]. To account for the vdW interactions in the case of bilayer VSSe, Grimme’s DFT-D3 [42] dispersion correction has been adopted. To avoid the interaction of the considered 2D VSSe structures with their periodic replicas, the length of  $c$  lattice parameter was set to 20 Å and 25 Å for the monolayer and bilayer, respectively. The convergence criterion for geometry optimization has been set to 0.01 eV/Å for the Hellmann-Feynman forces. The energy convergence threshold of  $10^{-5}$  eV has been set for the self-consistent-field iterations in solving the Kohn-Sham equations. The Monkhorst-Pack scheme [43] has been employed to perform the Brillouin zone integration, for which, the  $\mathbf{k}$ -mesh of the size  $12 \times 12 \times 1$  is employed for the geometry relaxation of the considered Janus VSSe monolayer and bilayers. Afterwards, the  $\mathbf{k}$ -mesh is refined to  $30 \times 30 \times 1$  for further calculations on the optimized monolayer and bilayers. The generalized gradient approximation (GGA) has been considered for the exchange-correlation functional. We start by using the Perdew-Burke-Ernzerhof (PBE) [44] version of the GGA for all the optimizations and to determine the structural properties of both the Janus VSSe monolayer and bilayers. Then, to better address the magnetic and electronic properties, we use the rotationally invariant DFT+ $U$  (GGA+ $U$ ) approach introduced by Liechtenstein *et al.* [45]. GGA+ $U$  is known to yield improved results as compared to GGA for the systems involving correlated electrons by taking into account the on-site Coulomb repulsion experienced by the localized electrons of  $d$  orbitals. The effective on-site interaction has been added to the  $3d$  electrons of vanadium by taking the Hubbard  $U$  parameter equal to 2.7 eV. The anisotropy of exchange interactions has been incorporated by taking Hund’s coupling  $J = 0.7$  eV. Our considered  $U$  and  $J$  values are consistent with the values used to study vanadium-based systems (non-Janus and Janus dichalcogenides) in earlier studies [21, 34, 46, 47]. The Bader charge analysis has been performed using a code developed by Henkelman group [48] to quantify the charges present on the involved atomic species.

The thermal stability of the VSSe bilayer was investigated by performing ab initio molecular dynamics (AIMD) simulations [49]. These simulations were conducted in the canonical ensemble using a Nosé-Hoover thermostat at two temperatures: room temperature (300 K) and an elevated temperature of 400 K. To determine the mechanical stability of the VSSe bilayer, the equilibrium lattice configuration has been subjected to small loading strains

ranging from -2 % to 2% in increments of 0.5 %. We focused on elastic deformations within the harmonic range in which the material exhibits a linear stress ( $\sigma$ ) response to the applied strain ( $\epsilon$ ), governed by the Hooke's law. This relation is expressed in the Voigt notation [50] and is given by

$$\sigma_i = \sum_{j=1}^6 C_{ij} \epsilon_j, \quad (1)$$

where  $\sigma_i$  and  $\epsilon_j$  represent the six independent components of the stress and strain vectors, respectively ( $1 \leq i, j \leq 6$ ), and  $C_{ij}$  is the second-order elastic stiffness tensor expressed as a  $6 \times 6$  symmetric matrix. The elastic energy  $\Delta E(V, \{\epsilon\})$  of a strained structure under the harmonic approximation, is defined as

$$\Delta E(V, \{\epsilon_i\}) = E(V, \{\epsilon_i\}) - E(V_0, 0) = \frac{V_0}{2} \sum_{i,j=1}^6 C_{ij} \epsilon_i \epsilon_j, \quad (2)$$

where  $E(V, \{\epsilon_i\})$  and  $E(V_0, 0)$  denote the total energies of the strained and unstrained crystal structures with volumes  $V$  and  $V_0$ , respectively. For 2D materials in the  $xy$ -plane, the stiffness tensor of Eq. 1 reduces to a  $3 \times 3$  symmetric matrix, which gives in-plane stiffness components  $C_{ij}$  with  $i, j = 1, 2, 6$ . These second order  $C_{ij}$  components are determined using the energy-strain relation as implemented in the VASPKIT package [51]. For a 2D hexagonal isotropic system in the  $xy$ -plane, the relations simplify to  $C_{61} = C_{16} = C_{62} = C_{26} = 0$ , leaving only two independent constants,  $C_{11}$  and  $C_{12}$  where  $C_{11} = C_{22}$ ,  $C_{21} = C_{12}$ , and  $C_{66} = 0.5 \times (C_{11} - C_{12})$ . Additionally, the direction-dependent Young's modulus  $E(\theta)$  and the Poisson's ratio  $\nu(\theta)$  were calculated using the following equations:

$$E(\theta) = \frac{C_{11}C_{22} - C_{12}^2}{C_{11} \sin^4 \theta + \left( \frac{C_{11}C_{22} - C_{12}^2}{C_{66}} - 2C_{12} \right) \sin^2 \theta \cos^2 \theta + C_{22} \cos^4 \theta}, \quad (3)$$

and

$$\nu(\theta) = \frac{C_{12}(\sin^4 \theta + \cos^4 \theta) - (C_{11} + C_{22} - \frac{C_{11}C_{22} - C_{12}^2}{C_{66}}) \sin^2 \theta \cos^2 \theta}{C_{11} \sin^4 \theta + \left( \frac{C_{11}C_{22} - C_{12}^2}{C_{66}} - 2C_{12} \right) \sin^2 \theta \cos^2 \theta + C_{22} \cos^4 \theta} \quad (4)$$

### III. RESULTS AND DISCUSSION

We started the calculations by optimizing the geometry of the VSSe monolayer. Next, we calculated the spin-polarized electronic band structure, density of states (DOS), and the

magnetic moments for the FM monolayer using the GGA+ $U$  approach, and found that our results are consistent with the previous studies [34]. More details about the crystal structure, electronic band structure, DOS, magnetic moments, and formation energy for the monolayer are provided in the Supplemental Material (SM) [52], and some references cited therein [53–55]. Next, we present and discuss results of our calculations on the bilayer.

### A. Stacking configurations and stability

In order to form the bilayer of VSSe, we stacked two geometry-optimized monolayers on top of each other in the following orders: (a) AA stacking (Fig. 1(a)) with the same type of atoms on both top and bottom layers, (b) AA' stacking (Fig. 1(b)) in which the top layer is anti-parallel to the bottom layer with V atoms vertically above the chalcogen atoms, S and Se of the bottom layer (and vice versa), and (c) finally AB stacking shown in Fig. 1(c) which is obtained by shifting the layers of AA' stacking. The AA stacked VSSe bilayer with broken inversion symmetry belongs to  $P\bar{3}m1$  space group and possesses the  $C_{3v}$  point group. In AA' stacking, a layer is rotated by  $180^\circ$  relative to another layer, which gives rise to a centrosymmetric bilayer if the two chalcogens are the same. However, in the case of VSSe, the two different chalcogens lead to the non-centrosymmetric AA' stacking. The AB stacking, which is also non-centrosymmetric, is obtained by shifting the layers of AA' stacking along the armchair direction such that V atoms of two layers are vertically above each other and the chalcogen of one layer lies on the top of the hexagon center of another layer. Due to the lack of inversion symmetry, both the AA' and AB stackings also belong to  $P\bar{3}m1$  space group, similar to the AA stacked VSSe bilayer. Thus, all three considered VSSe bilayers belong to the same space group as the monolayer. The AA' stacking type is normally observed in the bilayer of 2H-TMDs such as bilayer 2H-MoS<sub>2</sub> [56]. The monolayer of Janus 2H-VSSe has FM ordering in its ground state. When a bilayer composed of two such monolayers is formed, different magnetic orderings can be achieved with the change in the type of stacking leading to different ground states. For this purpose, we used  $2\times 2$  supercells consisting of 24 atoms, and built an FM and six possible antiferromagnetic (AFM) configurations considering various intra- and interlayer FM and AFM arrangements among V atoms. Further, supercells of various configurations are relaxed to obtain the optimized geometries including the interlayer distance corresponding to the ground state. The optimized FM and AFM configurations

(AFM1 to AFM6) are shown in Fig. S5 of SM [52], where a discussion on the nature of magnetic order of each configuration is also presented.

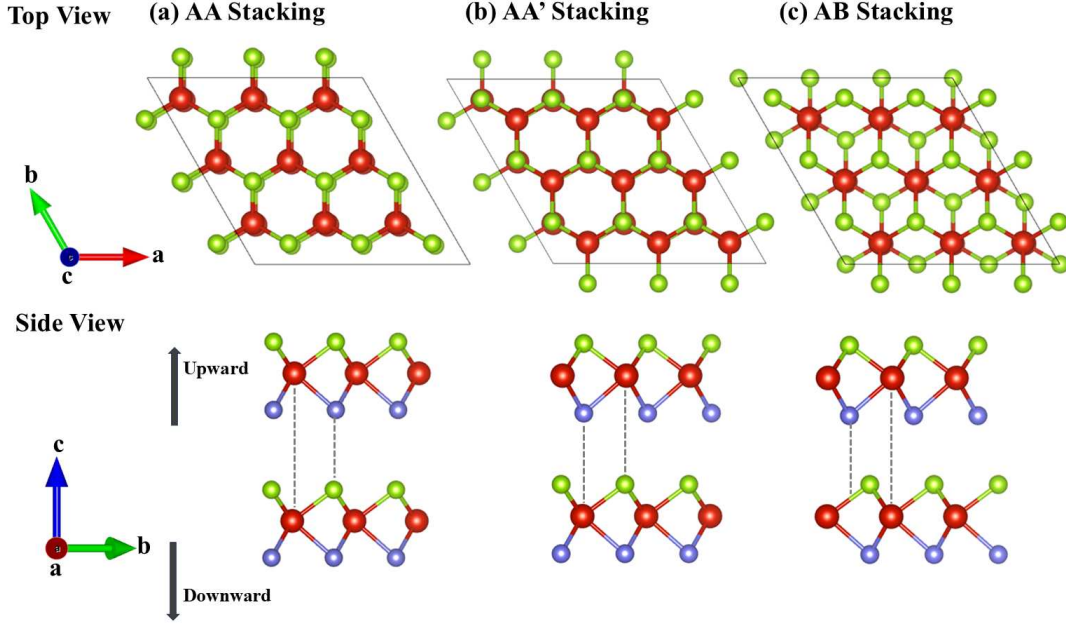


Figure 1. Considered stacking configurations of the bilayer of Janus VSSe. Red, green, and blue spheres represent the V, S, and Se atoms, respectively.

After optimization we found that FM ordering is favored as ground state in all three stacking configurations. The energy difference with respect to corresponding ground state,  $\Delta E$ , and interlayer distance,  $d$  (distance between two metal atoms of the top and bottom layers) after optimization for different stacking and magnetic configurations are given in Table I. The energy difference is calculated as  $\Delta E = E_{AFM} - E_{FM}$ , where,  $E_{FM}$  and  $E_{AFM}$  represent the total energies of the FM and different AFM configurations, respectively. The small energy difference ( $\sim 5$  meV) between FM and AFM1 configurations is obtained for each stacking because the two configurations differ only in their interlayer magnetic interactions which are weak, and the strong intralayer interactions in both cases are same (ferromagnetic). In contrast, other configurations, AFM2 – AFM6 involve antiferromagnetic interactions both interlayer and intralayer, leading to significantly larger energy differences relative to the FM configuration. The total energies of the three considered stacking configurations in the FM state follow the order:  $E_{AB} < E_{AA'} < E_{AA}$ . Among them, the AB stacking exhibits the lowest energy, indicating it is the most stable configuration. Based on this energy trend,



the relative stability of the stackings with FM ordering is:  $AB > AA' > AA$ . The trend in interlayer distance  $d$  is  $d_{AA} > d_{AA'} > d_{AB}$ , with the minimum  $d$  of 6.05 Å for the AB stacking. The interlayer distance shows the same trend as in the order of energies of different stackings for FM ordering. Following this, we proceed with a detailed investigation of the FM configuration of the AB stacked bilayer including the band gap tunability with respect to an external electric field.

Table I. Interlayer distance,  $d$ , and the relative energy,  $\Delta E$  of various magnetic configurations for different stackings.

Stacking $d$ (Å)			$\Delta E$ (meV per unit cell)						
			FM	AFM1	AFM2	AFM3	AFM4	AFM5	AFM6
AA	6.67	0	2.10	94.65	94.15	95.57	94.22	96.51	
AA'	6.20	0	3.38	100.40	100.00	101.83	100.45	104.36	
AB	6.05	0	4.59	94.39	92.61	92.89	92.03	93.33	

We calculated the layer binding energy,  $E_b$  as

$$E_b = E_{VSSe}^{AB} - 2E_{VSSe} \quad (5)$$

where  $E_{VSSe}$  and  $E_{VSSe}^{AB}$  represent the total energies of the considered FM VSSe monolayer and bilayer, respectively. The obtained  $E_b$  of -1.09 eV suggests the feasibility of bilayer formation in the AB stacking from the constituent monolayers. Further, to assess the thermal stability of the VSSe bilayer, we performed AIMD simulations in the canonical ensemble, employing the Nosé-Hoover thermostat [57]. The AIMD simulations were carried out separately at 300 K and 400 K, each for a total duration of 5 ps with a time step of 1 fs. Fig. 2 depicts the variation of the total energy over time for both the temperatures, and it is observed that there are minimal fluctuations in total energy (less than 0.1 eV) and minor changes in bond lengths, with the maximum variations of 0.11 Å and 0.10 Å for V-S and V-Se bonds, respectively, indicating the stability of the Janus VSSe bilayer at both the room temperature and elevated temperatures.

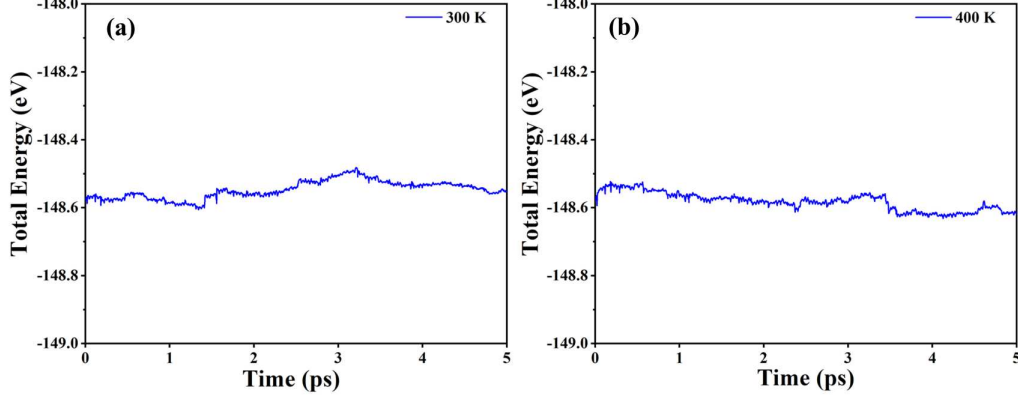


Figure 2. Total energy of the considered VSSe bilayer as a function of time at (a) 300 K and (b) 400 K.

## B. Mechanical properties

To evaluate the mechanical stability of the Janus VSSe bilayer, its mechanical properties were systematically investigated. Mechanical stability against structural deformation is critical, as lattice mismatch with a substrate can induce strain. Moreover, understanding mechanical properties is essential to assess the material's stiffness under external strain, as strain engineering serves as an effective method for tuning the properties of nanomaterials. To investigate these properties, the VSSe bilayer was subjected to small deformations with strains ranging from -2% to 2%, in increments of 0.5%. The total energy was calculated for each strain configuration, and the elastic stiffness constants were extracted by fitting the energy-strain curves using Eq. 2. The obtained elastic stiffness constants  $C_{11} = C_{22} = 215.21 \text{ Nm}^{-1}$ ,  $C_{21} = C_{12} = 78.43 \text{ Nm}^{-1}$ , and  $C_{66} = 68.39 \text{ Nm}^{-1}$  satisfy the Born-Huang criteria [58],  $C_{11}C_{22} - C_{12}^2 > 0$  and  $C_{66} > 0$ , confirming the mechanical stability of the Janus VSSe bilayer. Using the computed stiffness constants, additional mechanical properties were derived such as the shear modulus  $G$ , direction-dependent Young's modulus  $E(\theta)$ , and Poisson's ratio  $\nu(\theta)$ . The shear modulus  $G$  is generally equal to  $C_{66}$ , was determined to be  $68.39 \text{ Nm}^{-1}$ , indicating significant resistance of the VSSe bilayer to shear deformation. Further,  $E(\theta)$  and  $\nu(\theta)$  are determined using Eq. 3 and Eq. 4, with their respective polar plots depicted in Fig. 3(a) and Fig. 3(b). The computed results show isotropy in the mechanical behavior along parallel and perpendicular directions, with  $E(0^\circ) = E(90^\circ) = 186.62 \text{ Nm}^{-1}$  and  $\nu(0^\circ) =$

$\nu(90^\circ) = 0.36$ . This mechanical isotropy is further reflected in the uniform Young's modulus and Poisson's ratio across all directions in the  $xy$ -plane, consistent with the bilayer's isotropic crystal structure. The calculated Young's modulus for the Janus VSSe bilayer is lower than those reported for  $\text{MoS}_2$ ,  $\text{MoSe}_2$ ,  $\text{WS}_2$ ,  $\text{WSe}_2$ , and  $\text{WTe}_2$  bilayers but slightly higher than that of  $\text{MoTe}_2$  bilayer [59]. It also exceeds the values reported for non-magnetic Janus TMD monolayers ( $\text{MX}_2$ , where  $\text{M} = \text{Mo}, \text{W}$  and  $\text{X/Y} = \text{S}, \text{Se}, \text{and Te}$ ) [60]. For comparison, the theoretically calculated Young's modulus of the recently synthesized Janus  $\text{MoSSe}$  monolayer is  $123.43 \text{ Nm}^{-1}$  [60]. The positive Poisson ratio indicates that under tensile (compressive) strain in a direction, the bilayer expands (contracts) in the perpendicular direction, and its small value of  $\nu = 0.36$  suggests slight deformation. Overall, the analysis confirms the mechanical stability and isotropy of the Janus VSSe bilayer, making it a promising candidate for strain-engineered applications.

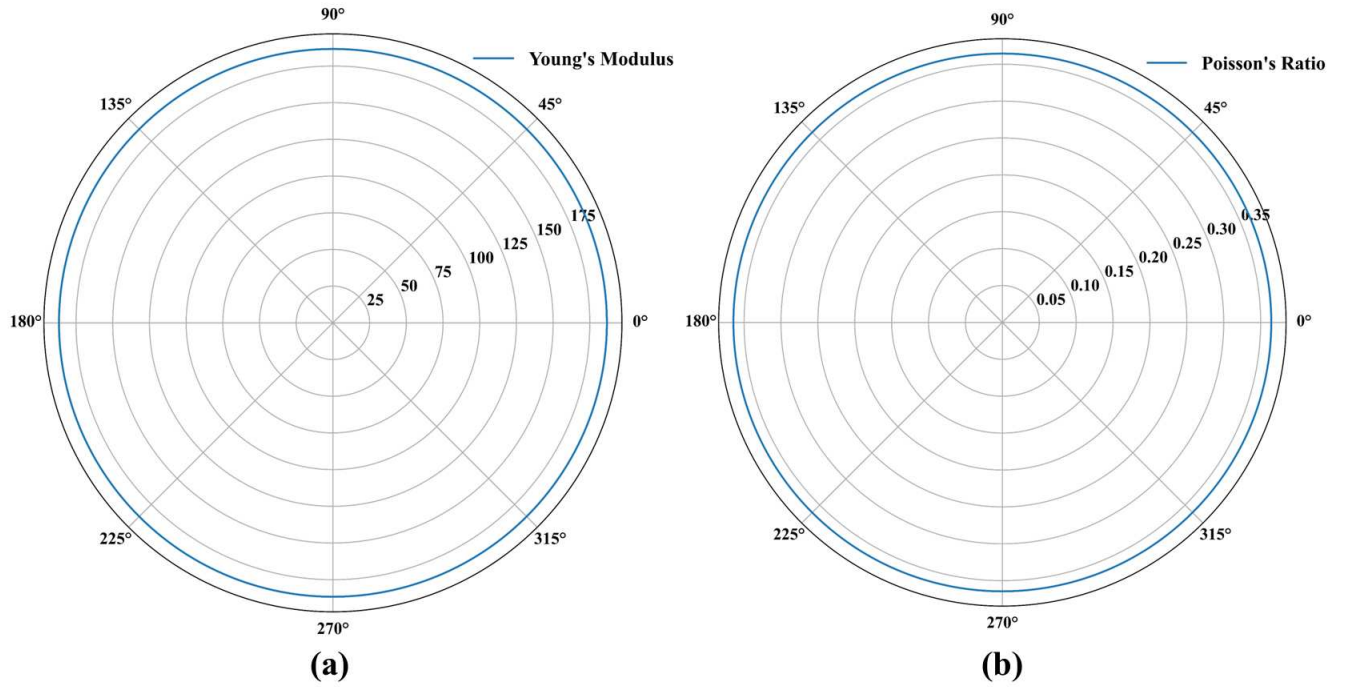


Figure 3. Orientation dependent (a) Young's Modulus  $E(\theta)$  in the units of  $\text{Nm}^{-1}$  and (b) Poisson ratio  $\nu(\theta)$  computed for the Janus VSSe bilayer.

The theoretical calculations of energetic, thermal, and mechanical stability support the feasibility of the synthesis of the Janus VSSe bilayer. Experimental realization of Janus  $\text{MoSSe}$  monolayer from its non-Janus counterparts,  $\text{MoS}_2$  and  $\text{MoSe}_2$  monolayers by thermal

selenization and sulphurization, respectively, have been reported in the literature [32, 61]. The monolayers of vanadium-based TMDs  $\text{VSe}_2$  and  $\text{VS}_2$  have already been synthesized experimentally [28, 62, 63]. Thus, the likelihood of synthesizing a Janus VSSe monolayer using similar experimental techniques appears promising. Subsequently, starting from the VSSe monolayers, corresponding bilayer can be obtained using the transfer techniques.

### C. Electronic structure and magnetic properties

#### 1. Electronic Structure

Now we present and discuss the electronic properties of the FM VSSe bilayer, calculated using the GGA+ $U$  method. From the computed spin-polarized band structure shown in Fig. 4(a) we note that, as compared to the monolayer, the magnitude of band gap ( $E_g$ ) for the bilayer gets significantly reduced to 0.11 eV and 0.60 eV for the majority and minority spin carriers, respectively. However, the positions corresponding to valence band maximum (VBM) and conduction band minimum (CBM) remain unaltered for both the spin orientations even after the formation of the bilayer, thus preserving the indirect nature of  $E_g$ . Interestingly, the energy states close to the Fermi level ( $E_F$ ) in both the valence and conduction band regions correspond to the same spin channel, i.e., the majority spin channel. This feature suggests a high probability of gap closing for majority spin bands compared to minority spin bands under the influence of an external perturbation, rendering the bilayer VSSe half-metallic. The 3D plots of the highest valence band and lowest conduction band corresponding to the majority spin carriers at  $k_z = 0$  plane are shown in Fig. S6 of the SM [52]. In order to see the contribution of atomic orbitals to the band structure, the atom-projected band structures corresponding to the outermost orbitals are presented in Figs. 4 (b) and (c), for the majority and minority spin orientations, respectively. It is observed that the bilayer resembles the monolayer VSSe in terms of the contribution of the involved atomic species to the CBM and VBM, corresponding to both the majority and minority spin carriers (See Fig. S3 of the SM [52] for atom-projected band structures of the monolayer). Furthermore, we show the spin-polarized atom-projected partial density of states (PDOS) in Fig. 5. The atoms of the bottom layer are labeled as V1, S1, and Se1, while those of the top layer are labeled as V2, S2, and Se2. It can be observed from Fig. 5 that VBM

has dominant top layer character (V2 ( $3d$ )) and CBM shows bottom layer characteristics (V1 ( $3d$ )) for the majority spin carriers. The CBM and VBM of minority spin carriers also possess the bottom and top layer characteristics, respectively, however, the Se2 ( $4p$ ) atom also contributes to VBM along with the V2 ( $3d$ ) atom. The contribution from different layers to the CBM and VBM of the spin channel close to the  $E_F$  is important for achieving FM semiconductor-to-half metal transition in the presence of external stimuli, as stated earlier. The majority spin channel of the considered VSSe bilayer satisfies this criterion as the contribution to CBM comes from the V( $3d$ ) atom of one layer, while the contribution to the VBM comes from the V ( $3d$ ) atom of another layer, thereby resulting in different layer characteristics. The total density of states (TDOS) plotted in the same figure (Fig. 5) is consistent with the calculated band structure of the VSSe bilayer.

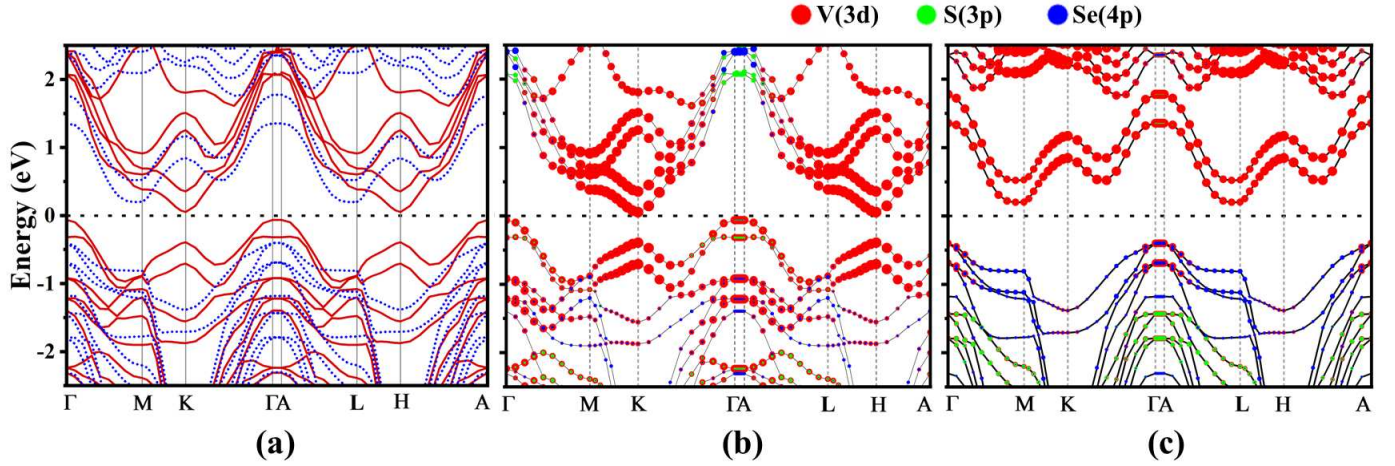


Figure 4. (a) Spin-polarized band structure, and projected band structures for (b) majority and (c) minority spin channels, of the VSSe bilayer. The solid red and dotted blue lines in (a) denote the energy states corresponding to the majority and minority spin channels, respectively. The dashed line at zero energy represents the Fermi energy,  $E_F$ .

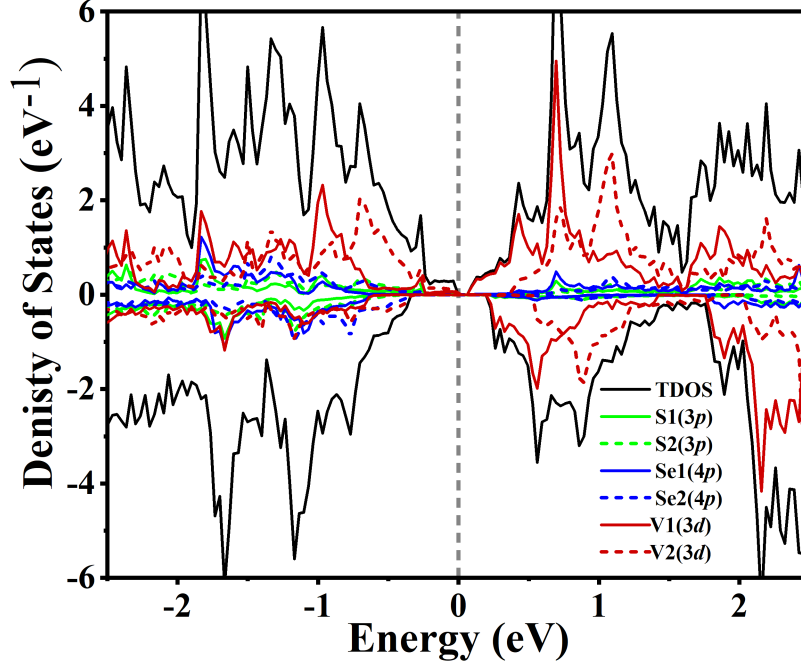


Figure 5. The spin-polarized TDOS and PDOS plotted for the considered FM Janus VSSe bilayer. 1 and 2 stand for the atomic species belonging to the bottom and top layers of the bilayer. The dashed line at zero energy represents  $E_F$ .

Similar to the VSSe monolayer, the structure of the VSSe bilayer shows a lack of horizontal mirror symmetry, and a difference in electronegativity between chalcogen atoms which can give rise to spontaneous polarization,  $\mathbf{P}$ , and an internal electric field  $\mathbf{E}_{\text{in}}$ . To illustrate the presence of the intrinsic electric field and polarization, we plotted the planar average of electrostatic potential energy perpendicular to the 2D surface, as a function of distance along  $z$ -direction (see Fig. 6). The asymmetric nature of the electrostatic potential energy for each layer indicates the presence of a non-vanishing  $\mathbf{E}_{\text{in}}$ . Further, the change in work function,  $\Delta\Phi = 9$  meV is also observed as we move from the lower layer to the upper one, consistent with the presence of  $\mathbf{E}_{\text{in}}$  and spontaneous polarization in the bilayer VSSe. Note that the value of  $\Delta\Phi$  in the case of the bilayer is more than that obtained for the monolayer case (5 meV). It is worth noting that the magnitude of  $\mathbf{P}$  increases with increasing  $\Delta\Phi$ . Therefore, the value of  $\mathbf{P}$  should be higher for the bilayer compared to the monolayer, and, indeed  $\mathbf{P}$  computed as dipole moment per unit area, is 0.04 and 0.05  $e/\text{nm}$ , for the mono- and bilayer, respectively. Furthermore,  $\mathbf{P}_{\text{bilayer}} > \mathbf{P}_{\text{monolayer}}$  is consistent with the fact that the bilayer has stronger  $\mathbf{E}_{\text{in}}$  as compared to the monolayer.

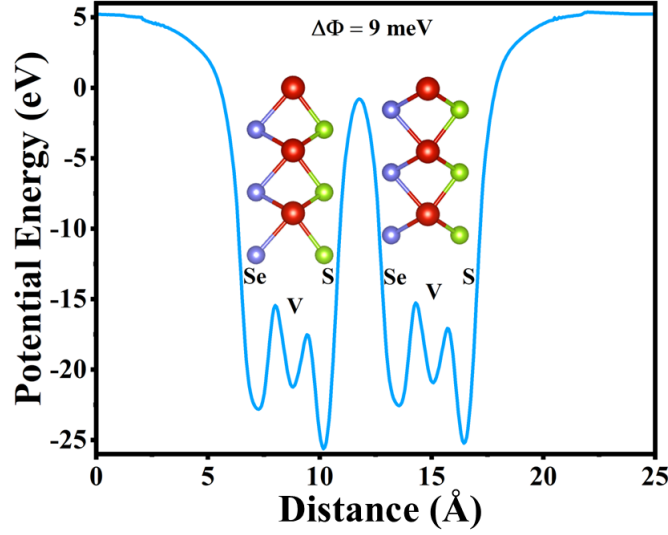


Figure 6. Planar average of the electrostatic potential energy as a function of distance in the  $z$ -direction, plotted for the VSSe bilayer under consideration.  $\Delta\Phi$  represents the change in work function and its non-zero value confirms the presence of inherent  $\mathbf{E}_{\text{in}}$ .

The Bader charge analysis has also been performed to see the amount of charge gain/loss by each atom in the bilayer, which is given in Table II. The negative and positive signs denote the gain and the loss of electrons, respectively. The table suggests that V atoms lose electrons, while, the chalcogen atoms gain electrons. The amount of electronic charge gained by each S atom is more compared to the Se atom due to the higher electronegativity of the former atom. This leads to a redistribution of the electronic charges and creation of an  $\mathbf{E}_{\text{in}}$  in the upward direction which is also in agreement with Fig. 6. The nature of bonding is also verified by computing the electron localization function (ELF) presented in Fig. 7, which takes the values between 0.0 and 1.0 denoting complete delocalization, and perfect localization of the electrons, respectively. A highly localized electronic charge distribution is found around the chalcogen atoms, with the delocalized electron density around the V atom. This is attributed to the higher electronegativity of the S/Se atoms compared to the V atom, thereby resulting in more ionic character of the V–S and V–Se bonds with partial covalent character as indicated by the green region (value 0.5) around them.

Table II. Charge gain/loss of each atomic species obtained using the Bader charge analysis in terms of charge of an electron ( $e$ ). Here positive and negative signs signify the electron loss and gain, respectively.

Layer 1			Layer 2		
V1	S1	Se1	V2	S2	Se2
1.25	-0.70	-0.55	1.24	-0.70	-0.54

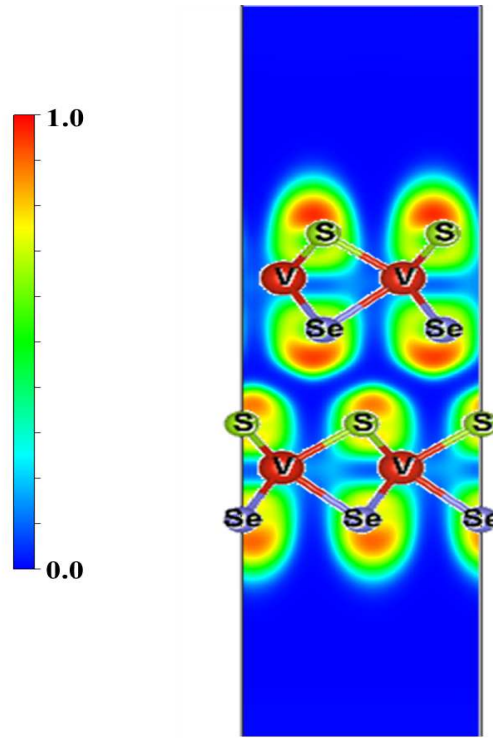


Figure 7. Electron localization function plot for the considered VSSe bilayer which shows the electronic distribution around atoms. The values 0.0 and 1.0 denote the fully delocalized and localized electronic charge distribution, respectively.

## 2. Magnetic Properties

The magnetic moments associated with each atomic species are computed using the GGA+ $U$  method, and their calculated values (see Table III) for the two V atoms, V1 and V2 in the bilayer are  $1.18 \mu_B$  and  $1.19 \mu_B$ , respectively, which are almost identical to  $1.18 \mu_B$  computed



for the monolayer. As anticipated, the primary contribution to magnetism comes from the transition metal atoms (V) of both the layers due to the unpaired electrons in  $d$  orbitals. Further, we computed the spin density difference defined as  $M(\vec{r}) = \rho_{\uparrow}(\vec{r}) - \rho_{\downarrow}(\vec{r})$ , where  $\rho_{\uparrow}(\vec{r})$  and  $\rho_{\downarrow}(\vec{r})$  signify the majority and minority spin densities, respectively, to understand the distribution of the magnetic moments on different atoms. From the  $M(\vec{r})$  plotted in Fig. 8 for our considered FM VSSe bilayer, it is clear that the spin density, which is contributed by the majority spin carriers, primarily resides on the vanadium atoms, consistent with their significant contribution to the overall magnetic moment. The ferromagnetism observed within the intra- and interlayer domains of the VSSe bilayer can be attributed to the indirect exchange coupling between the magnetic moments localized on vanadium, termed super-exchange (SE) [34]. Intralayer SE arises from V-S-V and V-Se-V coupling, while the interlayer SE stems from V-Se-S-V couplings. Further, the bond angles in the top and bottom layers of the VSSe bilayer are close to  $90^\circ$ , confirming the FM superexchange in the bilayer according to the Goodenough-Kanamoris rule [64]. Similar superexchange-based couplings have already been reported for the case of the monolayer [34]. Additionally, magnetic anisotropy calculations are performed to ascertain the easy-plane/axis of magnetization in the considered FM Janus VSSe bilayer, because the magnetic anisotropy significantly influences the stability of 2D ferromagnets. For example, Dey *et al.* [34] reported the easy-plane of magnetization to be the plane of the VSSe monolayer, with the spins oriented along it. We computed the magnetic anisotropy energy (MAE) as  $\text{MAE} = E_{[100]} - E_{[001]}$ , where  $E_{[100]}$  and  $E_{[001]}$  denote the energies corresponding to the in-plane and out-of-plane magnetization orientations, respectively. For the purpose, we employed the GGA+ $U$  approach, including the spin-orbit coupling to account for the relativistic effects, and obtained MAE to be -0.66 meV indicating that the FM Janus VSSe bilayer also manifests an easy plane of magnetization, which is the plane of the bilayer. This suggests that the intrinsic magnetic anisotropy of the VSSe monolayer persists even after bilayer formation, due to the weak nature of the vdW interaction holding the two layers together. Moreover, our MAE value for the VSSe bilayer is quite close to the corresponding value for the monolayer [34].

Table III. Localized magnetic moments (in the units of Bohr magneton,  $\mu_B$ ) on each of the constituent elements.

Method	Layer 1			Layer 2		
	V1	S1	Se1	V2	S2	Se2
GGA+ $U$	1.18	-0.08	-0.13	1.19	-0.08	-0.14

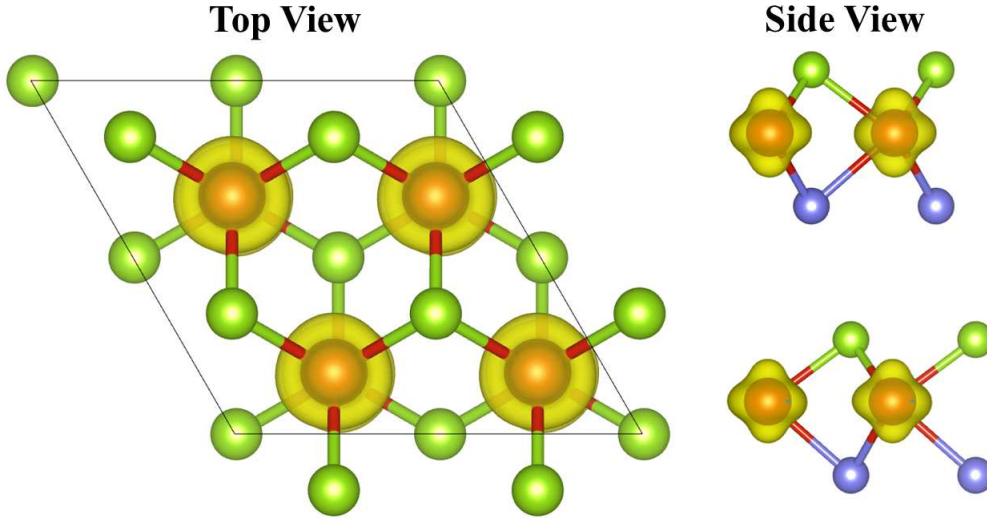


Figure 8. The calculated spin density difference for the VSSe bilayer under consideration, plotted at an isosurface value of  $0.0186 \text{ e}/\text{\AA}^3$ . The yellow color represents the spin density corresponding to majority spin carriers.

#### D. Effect of external electric field on the electronic properties

This section elucidates the effect of external electric field on the electronic properties of the FM Janus VSSe bilayer. As discussed in Sec. III C, the energy states close to  $E_F$  in both the valence band and conduction band regions correspond to the majority spin channel suggesting the possibility of gap closing under an external perturbation. This closing of one spin channel can lead to half-metallic behavior which can in turn be useful for applications in spintronics. Here we use an external electric field ( $\mathbf{E}_{\text{ex}}$ ) as a perturbation, to see the effect on the electronic structure and band gap of the VSSe bilayer.  $\mathbf{E}_{\text{ex}}$  is applied normal to the considered VSSe bilayer with its magnitude ranging from  $0.08 \text{ V}/\text{\AA}$  to  $0.50 \text{ V}/\text{\AA}$ , in both

the upward and downward directions, denoted by  $\mathbf{E}_{\text{ex}}^{\uparrow}$  and  $\mathbf{E}_{\text{ex}}^{\downarrow}$ , respectively. We observe that for both spin channels,  $E_g$  increases with increasing strengths of  $\mathbf{E}_{\text{ex}}^{\uparrow}$ , while, decreasing behavior in  $E_g$  is observed with increasing  $\mathbf{E}_{\text{ex}}^{\downarrow}$ . This observed change in  $E_g$  with direction and intensities of  $\mathbf{E}_{\text{ex}}$  is depicted in Fig. 9. The VSSe bilayer with the electric field applied upward can be useful in applications that demand narrow band gap semiconductors, such as adaptive radiation sensors and tunable IR photodetectors [65]. To investigate the effect of applied electric field on charge distribution, we plotted charge density difference for with and without  $\mathbf{E}_{\text{ex}}$  case, i.e.,  $\rho(\mathbf{E}_{\text{ex}}) - \rho(0)$ . The difference is plotted for an electric field of strength 0.18 V/Å applied in both the upward and downward directions, as shown in Fig. S7 of the SM [52]. It is observed that the charges accumulate at the top and bottom layers of the bilayer on applying  $\mathbf{E}_{\text{ex}}$  in the upward (Fig. S7(a)) and downward (see Fig. S7(b)) directions, respectively.

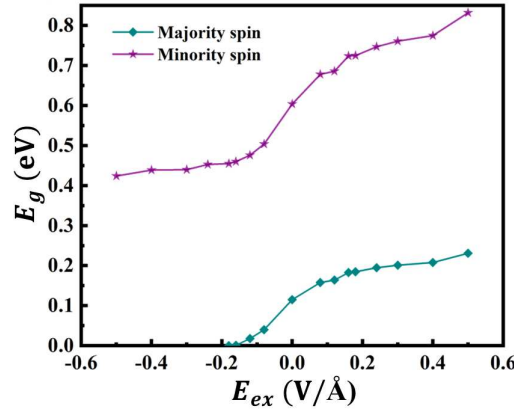


Figure 9. Variation of  $E_g$  with the strengths of applied  $\mathbf{E}_{\text{ex}}$ . The positive (negative) values of  $\mathbf{E}_{\text{ex}}$  imply it is in the upward (downward) direction, normal to the plane of considered VSSe bilayer.

We further explore the effect of  $\mathbf{E}_{\text{ex}}^{\downarrow}$ , as it leads to the lowering of the gap. The band structures for four varying strengths of  $\mathbf{E}_{\text{ex}}^{\downarrow}$  are presented in Fig. 10, from where it is obvious that the application of  $\mathbf{E}_{\text{ex}}^{\downarrow}$  results in gradual downward and upward shifts of the CBM and VBM, respectively, for both spin channels. However, the  $\mathbf{k}$ -point corresponding to the VBM and CBM for both spins remains unchanged upon applying  $\mathbf{E}_{\text{ex}}^{\downarrow}$ . The fundamental gap closes ( $E_g \rightarrow 0$ ) for the majority spin carriers at  $\mathbf{E}_{\text{ex}}^{\downarrow} = 0.16$  V/Å (Fig. 10(a)), with the CBM and VBM of the majority spin channel just touching each other, while a significant gap still exists for the minority spin carriers. Therefore, our calculations predict the considered

FM Janus VSSe bilayer to be a spin gapless semiconductor (SGS) at that field strength ( $\mathbf{E}_{\text{ex}}^{\downarrow} = 0.16 \text{ V/\AA}$ ). SGS is a subclass of conventional half-metallic ferromagnets, providing a new route to spintronics [66, 67]. When  $\mathbf{E}_{\text{ex}}^{\downarrow}$  is increased to  $0.18 \text{ V/\AA}$  (Fig. 10(b)), the CBM and VBM of majority spin crosses each other at  $E_F$  and a small overlap of about 9 meV between them (CBM and VBM) is observed. The overlap between the CBM and VBM corresponding to the majority spin channel increases further with increasing  $\mathbf{E}_{\text{ex}}^{\downarrow}$  ( $\geq 0.2 \text{ V/\AA}$ ), while a significant  $E_g$  still exists for the minority spin channel (see Fig. 10(c) and (d)). Therefore, a crossover from semiconducting to half-metallic behavior of the considered VSSe bilayer is achieved for  $\mathbf{E}_{\text{ex}}^{\downarrow} \geq 0.18 \text{ V/\AA}$ . This value of the required electric field is lower than the values reported for other systems to undergo semiconductor-to-half-metal transition. For instance, the half-metallic behavior reported for  $\text{CrI}_3\text{-CrGeTe}_3$  heterobilayer is at an external field of  $0.6 \text{ V/\AA}$  [19], while in the  $\text{CrSBr}$  monolayer, it has been reported at a field strength of  $0.3 - 0.4 \text{ V/\AA}$  [18]. Notably, the predicted electric field strength for the VSSe bilayer ( $\approx 0.18 \text{ V/\AA}$ ) is both smaller and practically feasible, as a study by Benjamin *et al.* [68] demonstrated the realization of an intense electric field larger than  $0.4 \text{ V/\AA}$  using dual ionic grating.

The resulting spin gapless ( $\mathbf{E}_{\text{ex}}^{\downarrow} = 0.16 \text{ V/\AA}$ ) and half-metallic ( $\mathbf{E}_{\text{ex}}^{\downarrow} \geq 0.18 \text{ V/\AA}$ ) behaviors can also be verified from the corresponding value of TDOS for the majority spin carriers at  $E_F$ . A small value of TDOS ( $0.33 \text{ eV}^{-1}$ ) at  $E_F$  favors the spin gapless nature for the case of  $\mathbf{E}_{\text{ex}}^{\downarrow}$  equaling  $0.16 \text{ V/\AA}$ . With the increasing  $\mathbf{E}_{\text{ex}}^{\downarrow}$ , a rise in the TDOS at  $E_F$  is observed. For the applied fields of  $0.18 \text{ V/\AA}$ ,  $0.20 \text{ V/\AA}$ , and  $0.30 \text{ V/\AA}$ , enhanced TDOS of magnitudes  $0.40$ ,  $0.44$ , and  $0.64 \text{ eV}^{-1}$  at  $E_F$  are obtained, respectively (See Fig. S8 of the SM for TDOS plots). For the resulting half-metallic VSSe bilayer (case of  $\mathbf{E}_{\text{ex}}^{\downarrow} = 0.18 \text{ V/\AA}$ ), the intrinsic spin polarization ( $P_s$ ) is calculated using the following formula

$$P_s = \frac{n_{\uparrow}(E_F) - n_{\downarrow}(E_F)}{n_{\uparrow}(E_F) + n_{\downarrow}(E_F)} \times 100 \quad (6)$$

where  $n_{\uparrow}(E_F)$  and  $n_{\downarrow}(E_F)$  represent the density of states at  $E_F$  for the majority and minority spin channels, respectively. Due to zero  $n_{\downarrow}(E_F)$ , 100 % intrinsic spin polarization is obtained which suggests that the VSSe bilayer can be explored for spintronics. It is worth mentioning that we also investigated the effect of external electric field on the band gap of VSSe monolayer, but no such change in the band gap is observed, clearly implying that the spin-gapless as well as half-metallic behaviors discussed above are unique properties of the

bilayer.

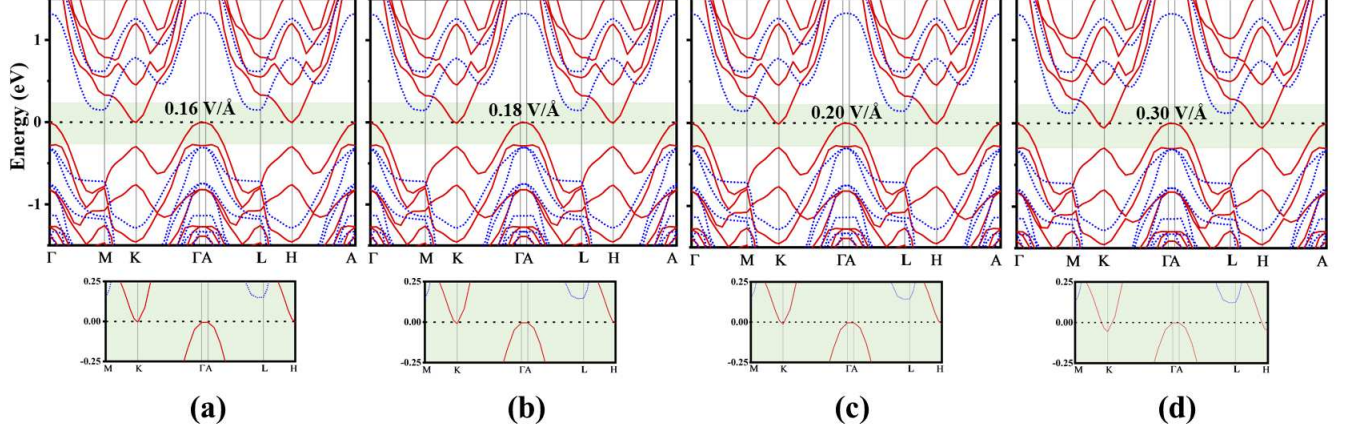


Figure 10. Spin-polarized band structures of the VSSe bilayer in the presence of four different  $\mathbf{E}_{\text{ex}}^{\downarrow}$  strengths. The dashed line at zero represents  $E_F$ .

To get a picture of the role of atomic orbitals in gap closing,  $l$  and  $m$  (azimuthal and magnetic quantum numbers) decomposed atom-projected PDOS are plotted corresponding to the majority spin carriers. The following two different cases corresponding to  $\mathbf{E}_{\text{ex}}^{\downarrow}$ : (a) no external electric field and (b) at  $\mathbf{E}_{\text{ex}}^{\downarrow} = 0.20 \text{ V/\AA}$  are considered, as depicted in Fig. 11 along with the respective band structures. The non-identical PDOS signatures of the two V atoms (V1 and V2), two S atoms (S1 and S2), and two Se atoms (Se1 and Se2) are due to broken horizontal mirror symmetry. For the pristine VSSe bilayer (Fig. 11(a)), VBM is composed primarily of the  $d_{z^2}$  orbital of V2 atom of top layer with a small contribution of the same orbital of V1 of bottom layer. Also, in the CBM, there is a small mixing of V1  $d_{xy}, d_{x^2-y^2}$  orbitals with the  $d_{z^2}$  orbital. Additionally,  $p_z$  orbitals of S1 and Se2 atoms make small contributions to VBM, whereas, a negligible contribution comes from the Se1 and S2 atoms as they do not interact with the  $p_z$  orbitals of the neighboring layers due to the presence of vacuum. With the increasing magnitude of  $\mathbf{E}_{\text{ex}}^{\downarrow}$ , the valence (conduction) band states exhibit upward (downward) shifts leading to the reduction of the band gap, and consequently, half metallicity as discussed earlier. The changes in the contribution from atomic orbitals for  $\mathbf{E}_{\text{ex}}^{\downarrow} = 0.20 \text{ V/\AA}$ , compared to the  $\mathbf{E}_{\text{ex}}^{\downarrow} = 0$  case, can be observed in the PDOS plot presented in Fig. 11(b). The redistribution of states of  $d_{z^2}$  orbitals around  $E_F$  indicates that the  $d_{z^2}$  orbitals of both the V atoms (V1 from CBM side and V2 from VBM side) primarily contribute to the closing of the gap. These results of the  $lm$ -decomposed

PDOS are also reflected in the band decomposed charge density distribution plotted for the CBM and VBM corresponding to the majority spin carriers in Fig. 12. Fig. 12 suggests: (a) in the absence of the external field, the contribution to CBM comes completely from the bottom layer, whereas, the top layer mainly contributes to the VBM with small participation from the bottom layer, and (b) at  $\mathbf{E}_{\text{ex}} = 0.2 \text{ V/\AA}$ , the VBM and CBM are mainly distributed over the top and bottom layers, respectively.

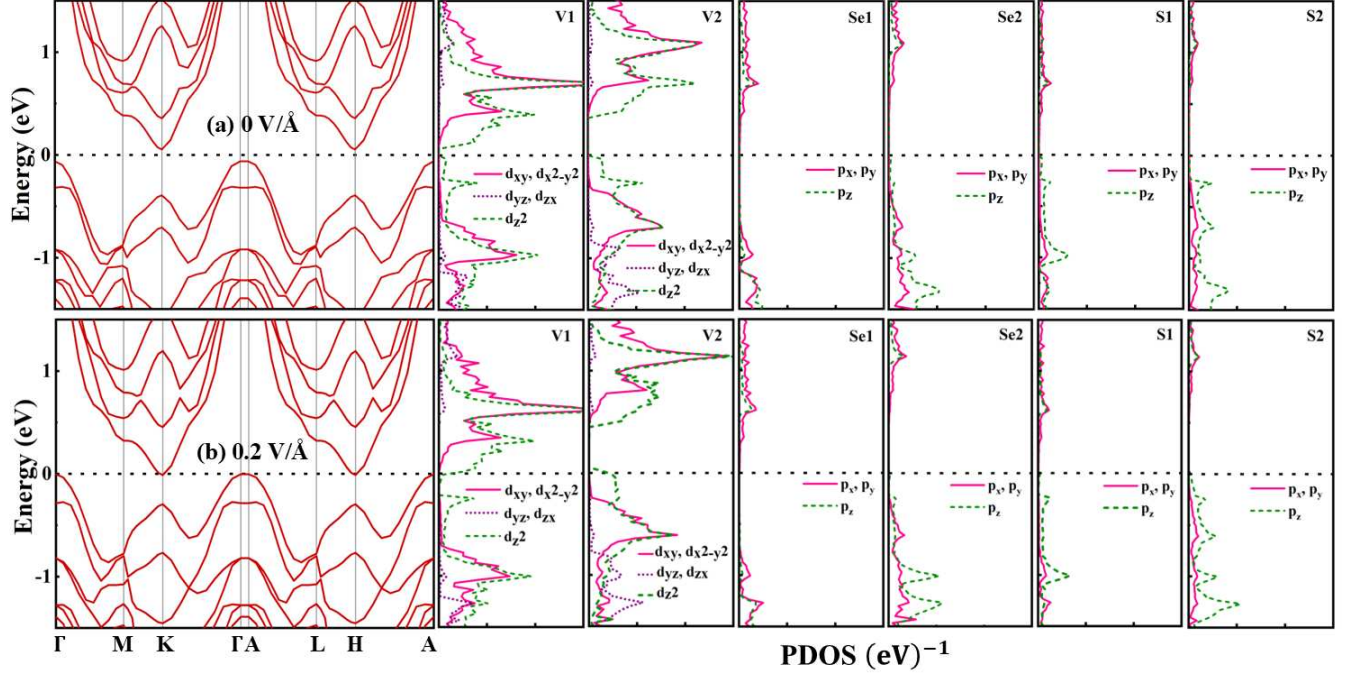


Figure 11. Band structure and  $lm$ -decomposed atom projected PDOS corresponding to the majority spin carriers of the VSSe bilayer when (a)  $\mathbf{E}_{\text{ex}}$  is absent and (b)  $\mathbf{E}_{\text{ex}}^{\downarrow} = 0.2 \text{ V/\AA}$ . The dashed line at zero represents  $E_F$ .



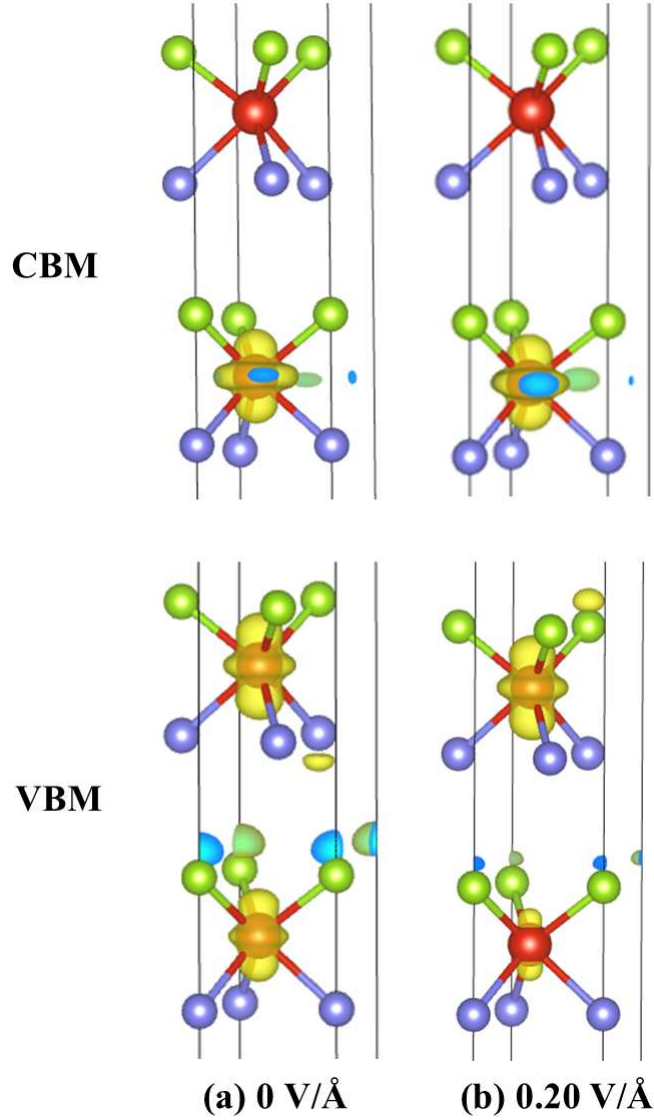


Figure 12. Charge density composition of the VBM and CBM corresponding to the majority spin carriers of the VSSe bilayer for cases: (a)  $\mathbf{E}_{\text{ex}}$  is absent and (b)  $\mathbf{E}_{\text{ex}}^{\downarrow} = 0.2 \text{ V/\AA}$ . All the plots are at an isosurface value of  $0.016 \text{ e/\AA}^3$ . The yellow and blue colors depict the charge accumulation and depletion regions, respectively.

In order to understand the static dielectric response of the VSSe bilayer, we calculated its electric polarization,  $\mathbf{P}_{\text{ex}}$ , for different values of the applied electric field, and the results are plotted in Fig. 13. A significant non-zero value of  $\mathbf{P}_{\text{ex}} = 0.49 \times 10^{-2} \text{ e/\AA}$  at  $\mathbf{E}_{\text{ex}} = 0$ , shows the spontaneous polarization which arises due to  $\mathbf{E}_{\text{in}}$  caused by the lack of mirror symmetry, as discussed earlier. Upon application of  $\mathbf{E}_{\text{ex}}$ , polarization increases monotonically with the

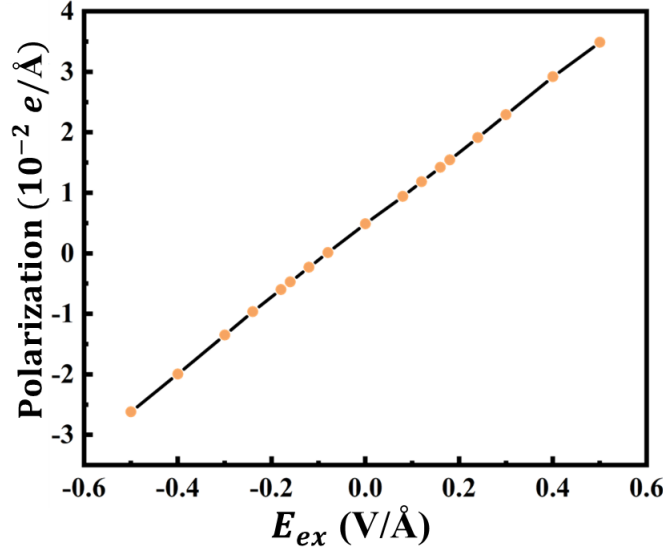


Figure 13. Electric polarization ( $\mathbf{P}_{\text{ex}}$ ) plotted as a function of  $\mathbf{E}_{\text{ex}}$ . The positive (negative) values of  $\mathbf{E}_{\text{ex}}$  imply it is in the upward (downward) direction, normal to the plane of considered VSSe bilayer.

strength of  $\mathbf{E}_{\text{ex}}^{\uparrow}$ , whereas, it decreases with the increase in strength of  $\mathbf{E}_{\text{ex}}^{\downarrow}$ . The reason for former is that  $\mathbf{E}_{\text{ex}}^{\uparrow}$  is applied along the direction of  $\mathbf{E}_{\text{in}}$ , while in the latter case the direction of  $\mathbf{E}_{\text{ex}}^{\downarrow}$  is opposite to that of  $\mathbf{E}_{\text{in}}$ . From these observations we infer that  $\mathbf{E}_{\text{ex}}^{\uparrow}$  strengthens the intrinsic dipole moment present in the bilayer structure, thereby increasing the corresponding polarization. However,  $\mathbf{E}_{\text{ex}}^{\downarrow}$  attempts to reorient the intrinsic dipole in the opposite direction, i.e., in the direction of  $\mathbf{E}_{\text{ex}}^{\downarrow}$ . This initially decreases the magnitude of the dipole moment and polarization from the intrinsic one, and then it increases in the opposite direction once the dipole aligns in this direction. Furthermore, the  $\mathbf{P}_{\text{ex}} - \mathbf{E}_{\text{ex}}$  plot of Fig. 13 is strictly linear, implying that the VSSe bilayer considered in this work behaves like a linear dielectric.

#### IV. CONCLUSION

In this work we explored the effects of external electric field on the electronic band structure of vanadium-based 2D Janus VSSe bilayer and its potential application in spintronics. The structural, mechanical, electronic and magnetic properties of the bilayer have been investigated. The study shows that the VSSe bilayer is a ferromagnetic semiconductor possessing



an easy-plane of magnetization when stacked in AB configuration with indirect band gaps of 0.11 eV and 0.60 eV for majority and minority spin carriers, respectively. When subjected to an external electric field perpendicular to the plane, applied in both upward and downward directions, the bilayer exhibits tunable electronic properties. Our findings reveal that the band gap decreases (increases) with the increasing external field downward (upward). Notably, a semiconductor to half-metal transition occurs at a field strength of  $\approx 0.18$  V/Å, applied downward, while a spin gapless semiconducting behavior is observed at 0.16 V/Å. These transitions to half-metallic and spin gapless states are driven by the closing of the band gap corresponding to the majority spin, primarily due to the interaction of the vanadium atom's out-of-plane  $d_{z^2}$  orbitals across both layers. Furthermore, VSSe bilayer exposed to an upward electric field can be used in radiation sensors and IR photodetectors for which narrow band gap semiconductors are well suited. The ability to tune the band gap and obtain semiconductor-to-half-metal transition or vice-versa by reversing the electric field direction demonstrates the versatility of the VSSe bilayer. Our study predicts Janus VSSe bilayer as a promising candidate for future spintronic devices.

### ACKNOWLEDGMENTS

One of the authors, K.D. acknowledges financial assistance from the Prime Minister Research Fellowship (PMRF ID-1302054), MHRD, India, and Space Time computational facility of Indian Institute of Technology Bombay. S.S.S. acknowledges the support through the Institute Post-Doctoral Fellowship (IPDF) of Indian Institute of Technology Bombay.

### DATA AVAILABILITY STATEMENT

Majority of the data is given in the main manuscript and Supplemental Material and the rest of the data will be available from the authors upon reasonable request.

- 
- [1] Ethan C. Ahn. 2D materials for spintronic devices. *npj 2D Materials and Applications*, 4(1):17, Jun 2020.

- [2] David L. Cortie, Grace L. Causer, Kirrily C. Rule, Helmut Fritzsche, Wolfgang Kreuzpaintner, and Frank Klose. Two-Dimensional Magnets: Forgotten History and Recent Progress towards Spintronic Applications. *Advanced Functional Materials*, 30(18):1901414, 2020.
- [3] Xiaolong Liu and Mark C. Hersam. 2D materials for quantum information science. *Nature Reviews Materials*, 4(10):669–684, Oct 2019.
- [4] Fanjunjie Han, Xu Yan, Fei Li, Hong Yu, Wenjing Li, Xin Zhong, Aitor Bergara, and Guochun Yang. Prediction of monolayer  $FeP_4$  with intrinsic half-metal ferrimagnetism above room temperature. *Phys. Rev. B*, 107:024414, Jan 2023.
- [5] Dechen Zhang, Azizur Rahman, Wei Qin, Xingxing Li, Ping Cui, Zengming Zhang, and Zhenyu Zhang. Prediction of  $MnSiTe_3$  as an intrinsic layered half-metal. *Phys. Rev. B*, 101:205119, May 2020.
- [6] Qiushi Yao, Jiayu Li, and Qihang Liu. Fragile symmetry-protected half metallicity in two-dimensional van der Waals magnets: A case study of monolayer  $FeCl_2$ . *Phys. Rev. B*, 104:035108, Jul 2021.
- [7] Qisheng Wu, Yehui Zhang, Qionghua Zhou, Jinlan Wang, and Xiao Cheng Zeng. Transition-Metal Dihydride Monolayers: A New Family of Two-Dimensional Ferromagnetic Materials with Intrinsic Room-Temperature Half-Metallicity. *The Journal of Physical Chemistry Letters*, 9(15):4260–4266, Aug 2018.
- [8] Michael Ashton, Dorde Gluhovic, Susan B. Sinnott, Jing Guo, Derek A. Stewart, and Richard G. Hennig. Two-Dimensional Intrinsic Half-Metals With Large Spin Gaps. *Nano Letters*, 17(9):5251–5257, Sep 2017.
- [9] Bing Wang, Yehui Zhang, Liang Ma, Qisheng Wu, Yilv Guo, Xiwen Zhang, and Jinlan Wang.  $MnX$  ( $X = P, As$ ) monolayers: a new type of two-dimensional intrinsic room temperature ferromagnetic half-metallic material with large magnetic anisotropy. *Nanoscale*, 11:4204–4209, 2019.
- [10] Qi Pei, Xiaocha Wang, Jijun Zou, and Wenbo Mi. Half-metallicity and spin-valley coupling in 5d transition metal substituted monolayer  $MnPSe_3$ . *J. Mater. Chem. C*, 6:8092–8098, 2018.
- [11] Emilio Scalise, Michel Houssa, Geoffrey Pourtois, Valery Afanas'ev, and André Stesmans. Strain-induced semiconductor to metal transition in the two-dimensional honeycomb structure of  $MoS_2$ . *Nano Research*, 5(1):43–48, Jan 2012.

- [12] Ashwin Ramasubramaniam, Doron Naveh, and Elias Towe. Tunable band gaps in bilayer transition-metal dichalcogenides. *Phys. Rev. B*, 84:205325, Nov 2011.
- [13] Qiang Yang, Liangzhi Kou, Xiaohui Hu, Yifeng Wang, Chunhua Lu, Arkady V Krashenninnikov, and Litao Sun. Strain robust spin gapless semiconductors/half-metals in transition metal embedded  $MoSe_2$  monolayer. *Journal of Physics: Condensed Matter*, 32(36):365305, jun 2020.
- [14] Zailin Yang and Jun Ni. Modulation of electronic properties of hexagonal boron nitride bilayers by an electric field: A first principles study. *Journal of Applied Physics*, 107(10):104301, 05 2010.
- [15] Le Zhang, Shanshan Chen, Xiangyang Chen, Zhizhen Ye, and Liping Zhu. Electric-field driven insulator-metal transition and tunable magnetoresistance in ZnO thin film. *Applied Physics Letters*, 112(15):153505, 04 2018.
- [16] Yichen Liu, San-Dong Guo, Yongpan Li, and Cheng-Cheng Liu. Two-Dimensional Fully Compensated Ferrimagnetism. *Phys. Rev. Lett.*, 134:116703, Mar 2025.
- [17] San-Dong Guo. Valley polarization in two-dimensional zero-net-magnetization magnets. *Applied Physics Letters*, 126(8):080502, 02 2025.
- [18] Hao-Tian Guo, San-Dong Guo, and Yee Sin Ang. Electric-field induced half-metallic properties in an experimentally synthesized CrSBr monolayer. *Phys. Chem. Chem. Phys.*, 25:30269–30275, 2023.
- [19] Cheng Tang, Lei Zhang, Stefano Sanvito, and Aijun Du. Electric-controlled half-metallicity in magnetic van der waals heterobilayer. *J. Mater. Chem. C*, 8:7034–7040, 2020.
- [20] Xidong Duan, Chen Wang, Anlian Pan, Ruqin Yu, and Xiangfeng Duan. Two-dimensional transition metal dichalcogenides as atomically thin semiconductors: opportunities and challenges. *Chem. Soc. Rev.*, 44:8859–8876, 2015.
- [21] Houlong L. Zhuang and Richard G. Hennig. Stability and magnetism of strongly correlated single-layer  $VS_2$ . *Phys. Rev. B*, 93:054429, Feb 2016.
- [22] Yandong Ma, Ying Dai, Meng Guo, Chengwang Niu, Yingtao Zhu, and Baibiao Huang. Evidence of the Existence of Magnetism in Pristine  $VX_2$  Monolayers ( $X = S, Se$ ) and Their Strain-Induced Tunable Magnetic Properties. *ACS Nano*, 6(2):1695–1701, Feb 2012.
- [23] Wei Chen, Jian-min Zhang, Yao-zhuang Nie, Qing-lin Xia, and Guang-hua Guo. Electronic structure and magnetism of  $MTe_2$  ( $M = Ti, V, Cr, Mn, Fe, Co$  and  $Ni$ ) monolayers. *Journal*

- of Magnetism and Magnetic Materials*, 508:166878, 2020.
- [24] N. D. Mermin and H. Wagner. Absence of Ferromagnetism or Antiferromagnetism in One- or Two-Dimensional Isotropic Heisenberg Models. *Phys. Rev. Lett.*, 17:1133–1136, Nov 1966.
  - [25] Bevin Huang, Genevieve Clark, Efrén Navarro-Moratalla, Dahlia R. Klein, Ran Cheng, Kyle L. Seyler, Ding Zhong, Emma Schmidgall, Michael A. McGuire, David H. Cobden, Wang Yao, Di Xiao, Pablo Jarillo-Herrero, and Xiaodong Xu. Layer-dependent ferromagnetism in a van der waals crystal down to the monolayer limit. *Nature*, 546(7657):270–273, Jun 2017.
  - [26] Cheng Gong, Lin Li, Zhenglu Li, Huiwen Ji, Alex Stern, Yang Xia, Ting Cao, Wei Bao, Chenzhe Wang, Yuan Wang, Z. Q. Qiu, R. J. Cava, Steven G. Louie, Jing Xia, and Xiang Zhang. Discovery of intrinsic ferromagnetism in two-dimensional van der waals crystals. *Nature*, 546(7657):265–269, Jun 2017.
  - [27] Dante J. O’Hara, Tiancong Zhu, Amanda H. Trout, Adam S. Ahmed, Yunqiu Kelly Luo, Choong Hee Lee, Mark R. Brenner, Siddharth Rajan, Jay A. Gupta, David W. McComb, and Roland K. Kawakami. Room Temperature Intrinsic Ferromagnetism in Epitaxial Manganese Selenide Films in the Monolayer Limit. *Nano Letters*, 18(5):3125–3131, May 2018.
  - [28] Manuel Bonilla, Sadhu Kolekar, Yujing Ma, Horacio Coy Diaz, Vijaysankar Kalappattil, Raja Das, Tatiana Eggers, Humberto R. Gutierrez, Manh-Huong Phan, and Matthias Batzill. Strong room-temperature ferromagnetism in  $VSe_2$  monolayers on van der Waals substrates. *Nature Nanotechnology*, 13(4):289–293, Apr 2018.
  - [29] Tao Hu, Fanhao Jia, Guodong Zhao, Jiongyao Wu, Alessandro Stroppa, and Wei Ren. Intrinsic and anisotropic Rashba spin splitting in Janus transition-metal dichalcogenide monolayers. *Phys. Rev. B*, 97:235404, Jun 2018.
  - [30] Anders C. Riis-Jensen, Thorsten Deilmann, Thomas Olsen, and Kristian S. Thygesen. Classifying the Electronic and Optical Properties of Janus Monolayers. *ACS Nano*, 13(11):13354–13364, Nov 2019.
  - [31] Chunmei Zhang, Yihan Nie, Stefano Sanvito, and Aijun Du. First-Principles Prediction of a Room-Temperature Ferromagnetic Janus VSSe Monolayer with Piezoelectricity, Ferroelasticity, and Large Valley Polarization. *Nano Letters*, 19(2):1366–1370, Feb 2019.
  - [32] Jing Zhang, Shuai Jia, Iskandar Kholmanov, Liang Dong, Dequan Er, Weibing Chen, Hua Guo, Zehua Jin, Vivek B. Shenoy, Li Shi, and Jun Lou. Janus Monolayer Transition-Metal Dichalcogenides. *ACS Nano*, 11(8):8192–8198, Aug 2017.

- [33] Junjie He and Shuo Li. Two-dimensional Janus transition-metal dichalcogenides with intrinsic ferromagnetism and half-metallicity. *Computational Materials Science*, 152:151–157, 2018.
- [34] Dibyendu Dey and Antia S. Botana. Structural, electronic, and magnetic properties of vanadium-based Janus dichalcogenide monolayers: A first-principles study. *Phys. Rev. Mater.*, 4:074002, Jul 2020.
- [35] Chaobo Luo, Xiangyang Peng, Jinfeng Qu, and Jianxin Zhong. Valley degree of freedom in ferromagnetic Janus monolayer H-VSSe and the asymmetry-based tuning of the valleytronic properties. *Phys. Rev. B*, 101:245416, Jun 2020.
- [36] Georg Kresse and Jürgen Furthmüller. Efficiency of ab-initio total energy calculations for metals and semiconductors using a plane-wave basis set. *Comput. Mater. Sci.*, 6:15–50, 1996.
- [37] Georg Kresse and Jürgen Furthmüller. Efficient iterative schemes for ab initio total-energy calculations using a plane-wave basis set. *Phys. Rev. B*, 54:11169–11204, 1996.
- [38] Pierre Hohenberg and Walter Kohn. Inhomogeneous electron gas. *Phys. Rev.*, 136–143:B864, 1964.
- [39] Walter Kohn and Lu Jeu Sham. Self-consistent equations including exchange and correlation effects. *Phys. Rev.*, 140:A1133–A1138, 1965.
- [40] Georg Kresse and Daniel Joubert. From ultrasoft pseudopotentials to the projector augmented-wave method. *Phys. Rev. B*, 59:1758–1775, 1999.
- [41] Peter E Blöchl. Projector augmented-wave method. *Phys. Rev. B*, 50:17953–17979, 1994.
- [42] Stefan Grimme, Jens Antony, Stephan Ehrlich, and Helge Krieg. A consistent and accurate ab initio parametrization of density functional dispersion correction (DFT-D) for the 94 elements H-Pu. *J. Chem. Phys.*, 132:154104–154123, 2010.
- [43] Hendrik J Monkhorst and James D Pack. Special points for Brillouin-zone integrations. *Phys. Rev. B*, 13:5188–5192, 1976.
- [44] John P Perdew, Kieron Burke, and Matthias Ernzerhof. Generalized gradient approximation made simple. *Phys. Rev. Lett.*, 77:3865–3868, 1996.
- [45] A. I. Liechtenstein, V. I. Anisimov, and J. Zaanen. Density-functional theory and strong interactions: Orbital ordering in Mott-Hubbard insulators. *Phys. Rev. B*, 52:R5467–R5470, Aug 1995.
- [46] Fengyu Li, Kaixiong Tu, and Zhongfang Chen. Versatile Electronic Properties of  $VSe_2$  Bulk, Few-Layers, Monolayer, Nanoribbons, and Nanotubes: A Computational Exploration. *The*

- Journal of Physical Chemistry C*, 118(36):21264–21274, Sep 2014.
- [47] F. Aryasetiawan, K. Karlsson, O. Jepsen, and U. Schönberger. Calculations of Hubbard  $U$  from first-principles. *Phys. Rev. B*, 74:125106, Sep 2006.
  - [48] W Tang, E Sanville, and G Henkelman. A grid-based Bader analysis algorithm without lattice bias. *J. Phys. Condens. Matter*, 21:084204, 2009.
  - [49] G. Kresse and J. Hafner. Ab initio molecular-dynamics simulation of the liquid-metal–amorphous-semiconductor transition in germanium. *Phys. Rev. B*, 49:14251–14269, May 1994.
  - [50] R. C. Andrew, R. E. Mapasha, A. M. Ukpong, and N. Chetty. Mechanical properties of graphene and boronitrene. *Phys. Rev. B*, 85:125428, Mar 2012.
  - [51] Vei Wang, Nan Xu, Jin-Cheng Liu, Gang Tang, and Wen-Tong Geng. VASPKIT: A user-friendly interface facilitating high-throughput computing and analysis using VASP code. *Computer Physics Communications*, 267:108033, 2021.
  - [52] See Supplemental Material at [] for the detailed structural, electronic, and magnetic properties of Janus VSSe monolayer. For the VSSe bilayer, different magnetic configurations, its 3D band structure, charge density difference, and total density of states plots are presented.
  - [53] Shengmei Qi, Jiawei Jiang, and Wenbo Mi. Tunable valley polarization, magnetic anisotropy and Dzyaloshinskii–Moriya interaction in two-dimensional intrinsic ferromagnetic Janus 2H-VSeX ( $X = \text{S, Te}$ ) monolayers. *Phys. Chem. Chem. Phys.*, 22:23597–23608, 2020.
  - [54] A. H. M. Abdul Wasey, Soubhik Chakrabarty, and G. P. Das. Quantum size effects in layered  $VX_2$  ( $X = \text{S, Se}$ ) materials: Manifestation of metal to semimetal or semiconductor transition. *Journal of Applied Physics*, 117(6):064313, 02 2015.
  - [55] Jun Wang, Haibo Shu, Tianfeng Zhao, Pei Liang, Ning Wang, Dan Cao, and Xiaoshuang Chen. Intriguing electronic and optical properties of two-dimensional Janus transition metal dichalcogenides. *Phys. Chem. Chem. Phys.*, 20:18571–18578, 2018.
  - [56] Jiangang He, Kerstin Hummer, and Cesare Franchini. Stacking effects on the electronic and optical properties of bilayer transition metal dichalcogenides  $\text{MoS}_2$ ,  $\text{MoSe}_2$ ,  $\text{WS}_2$ , and  $\text{WSe}_2$ . *Phys. Rev. B*, 89:075409, Feb 2014.
  - [57] Shuichi Nosé. A unified formulation of the constant temperature molecular dynamics methods. *The Journal of Chemical Physics*, 81(1):511–519, 07 1984.
  - [58] Max Born, Kun Huang, and M. Lax. Dynamical Theory of Crystal Lattices. *American Journal of Physics*, 23(7):474–474, 10 1955.

- [59] Fan Zeng, Wei-Bing Zhang, and Bi-Yu Tang. Electronic structures and elastic properties of monolayer and bilayer transition metal dichalcogenides  $MX_2$  (M= Mo, W; X= O, S, Se, Te): a comparative first-principles study. *Chinese Physics B*, 24(9):097103, 2015.
- [60] Vuong Van Thanh, Nguyen Duy Van, Do Van Truong, Riichiro Saito, and Nguyen Tuan Hung. First-principles study of mechanical, electronic and optical properties of Janus structure in transition metal dichalcogenides. *Applied Surface Science*, 526:146730, 2020.
- [61] Ang-Yu Lu, Hanyu Zhu, Jun Xiao, Chih-Piao Chuu, Yimo Han, Ming-Hui Chiu, Chia-Chin Cheng, Chih-Wen Yang, Kung-Hwa Wei, Yiming Yang, Yuan Wang, Dimosthenis Sokaras, Dennis Nordlund, Peidong Yang, David A. Muller, Mei-Yin Chou, Xiang Zhang, and Lain-Jong Li. Janus monolayers of transition metal dichalcogenides. *Nature Nanotechnology*, 12(8):744–749, Aug 2017.
- [62] P. Chen, Woei Wu Pai, Y.-H. Chan, V. Madhavan, M. Y. Chou, S.-K. Mo, A.-V. Fedorov, and T.-C. Chiang. Unique Gap Structure and Symmetry of the Charge Density Wave in Single-Layer VSe<sub>2</sub>. *Phys. Rev. Lett.*, 121:196402, Nov 2018.
- [63] Camiel van Efferen, Joshua Hall, Nicolae Atodiresei, Virginia Boix, Affan Safeer, Tobias Wekking, Nikolay A. Vinogradov, Alexei B. Preobrajenski, Jan Knudsen, Jeison Fischer, Wouter Jolie, and Thomas Michely. 2D Vanadium Sulfides: Synthesis, Atomic Structure Engineering, and Charge Density Waves. *ACS Nano*, 18(22):14161–14175, Jun 2024.
- [64] John B Goodenough. Goodenough-Kanamori rule. *Scholarpedia*, 3(10):7382, 2008.
- [65] Jiajia Zha, Mingcheng Luo, Ming Ye, Tanveer Ahmed, Xuechao Yu, Der-Hsien Lien, Qiyuan He, Dangyuan Lei, Johnny C. Ho, James Bullock, Kenneth B. Crozier, and Chaoliang Tan. Infrared Photodetectors Based on 2D Materials and Nanophotonics. *Advanced Functional Materials*, 32(15):2111970, 2022.
- [66] X. L. Wang. Proposal for a New Class of Materials: Spin Gapless Semiconductors. *Phys. Rev. Lett.*, 100:156404, Apr 2008.
- [67] Zengji Yue, Zhi Li, Lina Sang, and Xiaolin Wang. Spin-Gapless Semiconductors. *Small*, 16(31):1905155, 2020.
- [68] Benjamin I Weintrub, Yu-Ling Hsieh, Sviatoslav Kovalchuk, Jan N Kirchhof, Kyrilo Greben, and Kirill I Bolotin. Generating intense electric fields in 2D materials by dual ionic gating. *Nat Commun*, 13(1):6601, November 2022.

# Supplemental Material for Electric field induced half-metallicity in a two-dimensional ferromagnetic Janus VSSe bilayer

Khushboo Dange,<sup>\*</sup> Shivprasad S. Shastri,<sup>†</sup> and Alok Shukla<sup>‡</sup>

*Department of Physics, Indian Institute of Technology Bombay, Powai, Mumbai 400076, India*

## A. Ferromagnetic (FM) Janus 2H-VSSe Monolayer

### 1. Structural Properties

The Janus VSSe monolayer has been theoretically predicted to exhibit intrinsic 2D ferromagnetism, with FM order primarily contributed by the V-3d electrons [1, 2]. Similar to non-Janus TMDs, two structural forms of the Janus VSSe monolayer have been predicted: (a) trigonal prismatic (2H) and (b) octahedral (1T), with the 2H-phase being energetically most stable [2]. Both the 2H and 1T phases of VSSe monolayer have  $P3m1$  space group. The crystal structure of the 2H polymorph of the VSSe monolayer possessing  $C_{3v}$  symmetry is depicted in Fig. S1. The Wyckoff position of vanadium atom is  $1a$  (0, 0,  $z$ ) and of chalcogens is  $1c$  ( $2/3$ ,  $1/3$ ,  $z$ ). The optimized in-plane lattice constant of the considered 2H-VSSe monolayer is 3.25 Å, consistent with the reported ones [3], and lies between the lattice constant of VS<sub>2</sub> (3.12 Å) and VSe<sub>2</sub> (3.33 Å) monolayers [4, 5]. The V-S and V-Se bond lengths are 2.37 Å and 2.51 Å, respectively, consistent with the reported values [3], and are in agreement with the size of the anions i.e.,  $r_S < r_{Se}$  ( $r$  denotes the ionic radius). To predict the energetic stability of the considered Janus VSSe monolayer, we have estimated its formation energy ( $E_f^{mono}$ ) using Eq. 1 by assuming that 2D Janus VSSe can be derived from VS<sub>2</sub> and VSe<sub>2</sub>.

$$E_f^{mono} = E_{VSSe} - \frac{1}{2}(E_{VS_2} + E_{VSe_2}) \quad (1)$$

where  $E_{VS_2}$ ,  $E_{VSe_2}$ , and  $E_{VSSe}$  are the energies of the optimized VS<sub>2</sub>, VSe<sub>2</sub>, and VSSe monolayers. These energies and the resultant  $E_f^{mono}$  are reported in Table S1 in the units of eV per formula unit (eV/f.u.). Our calculated negative formation energy (-0.046 eV/f.u.)

---

<sup>\*</sup> khushboodange@gmail.com

<sup>†</sup> shastri1992@gmail.com

<sup>‡</sup> shukla@iitb.ac.in



suggests that the Janus VSSe monolayer can be formed in equilibrium environment. We note that Luo *et al.* [6] also reported a negative formation energy of -0.00263 eV/f.u., which is about an order of magnitude smaller than our value. For comparison, we consider the case of Janus MoSSe monolayer which has been synthesized experimentally [7], although its formation energy has been computed to have a positive value of 0.02699 eV by Luo *et al.* [6]. Therefore, according to our calculations, VSSe monolayer can also be synthesized, because it is predicted to be more stable as compared to MoSSe. The cohesive energy per atom,  $E_c^{mono}$  is also calculated using the formula

$$E_c^{mono} = \frac{1}{3} (E_{VSSe} - (E_V + E_S + E_{Se})) \quad (2)$$

where  $E_V$ ,  $E_S$ , and  $E_{Se}$  represent the energies of the isolated V, S, and Se atoms, respectively. The resultant  $E_c^{mono}$  of -4.56 eV is about twice of that reported for the MoSSe monolayer (-2.32 eV) [8], and thus hints at the thermodynamic stability of the 2D Janus VSSe structure. Furthermore, its dynamic stability has already been confirmed in various studies through ab initio molecular dynamics (AIMD) simulations [6], as well as by the absence of imaginary frequencies in the phonon dispersion [1, 2, 6].

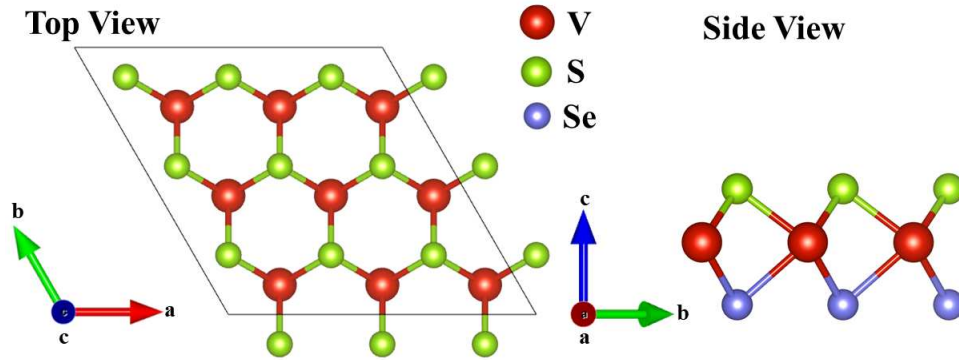


Figure S1. Crystal structure of the 2H polymorph of the Janus VSSe monolayer.

Table S1. Total energies (eV/f.u.) of the involved systems, formation energy,  $E_f^{mono}$  (eV/f.u.), and cohesive energy per atom,  $E_c^{mono}$  (eV) of the monolayer VSSe.

$E_{VS_2}$	$E_{VSe_2}$	$E_{VSSe}$	$E_f^{mono}$	$E_c^{mono}$
-19.703	-17.990	-18.892	-0.046	-4.560

## 2. Magnetic Moments

We computed the magnetic moments associated with each atomic species using the GGA+ $U$  method. The resultant magnetic moments associated with S, Se, and V atoms are  $-0.08\mu_B$ ,  $-0.14\mu_B$ , and  $1.19\mu_B$ , respectively, which are consistent with the reported values [2].

## 3. Electronic Properties

The electronic band structure simulations are performed within the spin-polarized formalism for the considered FM Janus VSSe monolayer using the GGA+ $U$  method, and the results are presented in Fig. S2(a). The band gaps ( $E_g$ ) of 0.57 eV and 0.88 eV are obtained for the majority and minority spin carriers, respectively. It is to be noted that the valence band maximum (VBM) for both the spin carriers is positioned at the same high symmetry point, i.e.,  $\Gamma$ , whereas, the conduction band minima (CBM) occur at different  $\mathbf{k}$ -points. For the majority (minority) spins, CBM is positioned at  $K$  (close to  $L$  along  $L \rightarrow A$ ), and thus an indirect  $E_g$  results for both the spin carriers. Our calculated band structure agrees well with that reported in the literature [2]. The total density of states (TDOS) and atom-projected partial density of states (PDOS) decomposed by azimuthal quantum number ( $l$ ) are also computed, as depicted in Fig. S2(b). The asymmetric nature of the DOS can be observed for the FM ground state of the Janus VSSe monolayer. The PDOS suggests that the CBM of both spin carriers comprises mainly of V-3d orbitals. The VBM corresponding to majority spin carriers is mainly composed of V-3d orbitals, whereas, the hybridization of the Se-4p and V-3d orbitals is involved in the VBM of minority states. The atom-projected  $l$ -decomposed band structures are also presented in Fig. S3. This plot supports the orbital characters of the VBM and CBM as shown by the PDOS plot.

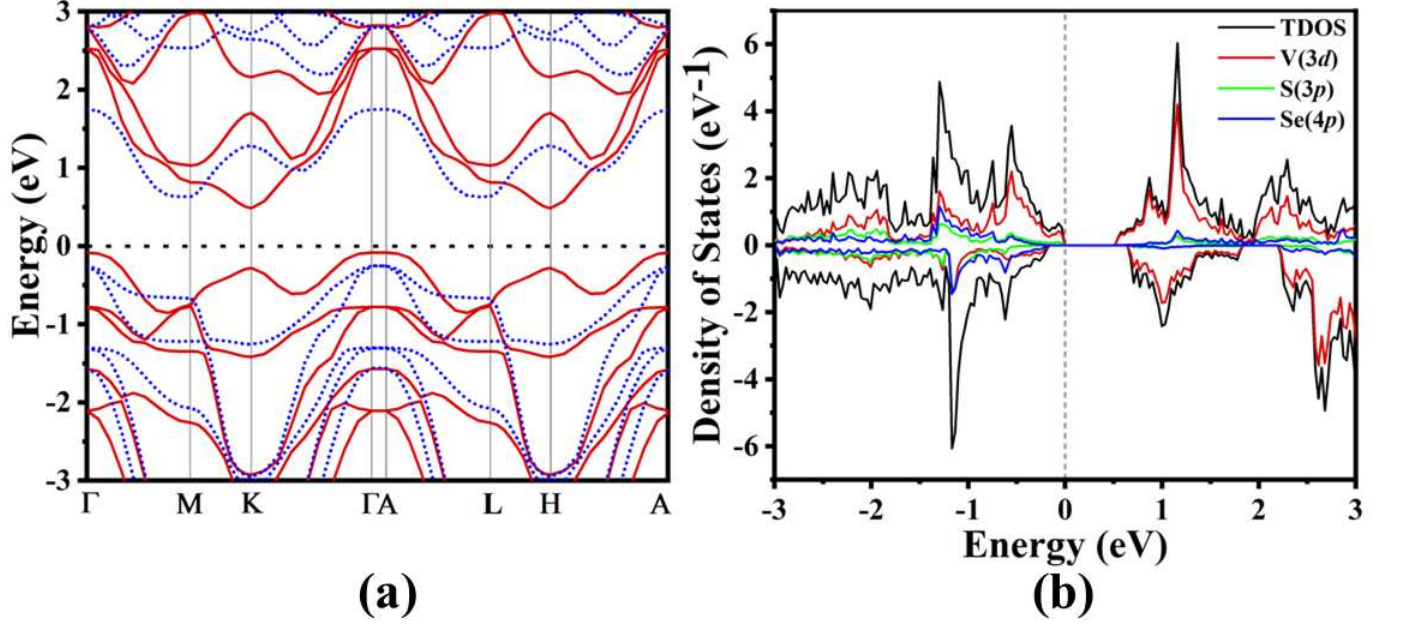


Figure S2. (a) Electronic band structure and (b) density of states (DOS) computed for the FM Janus VSSe monolayer. The solid red and dotted blue lines in (a) represent the energy states corresponding to the majority and minority charge carriers, respectively.

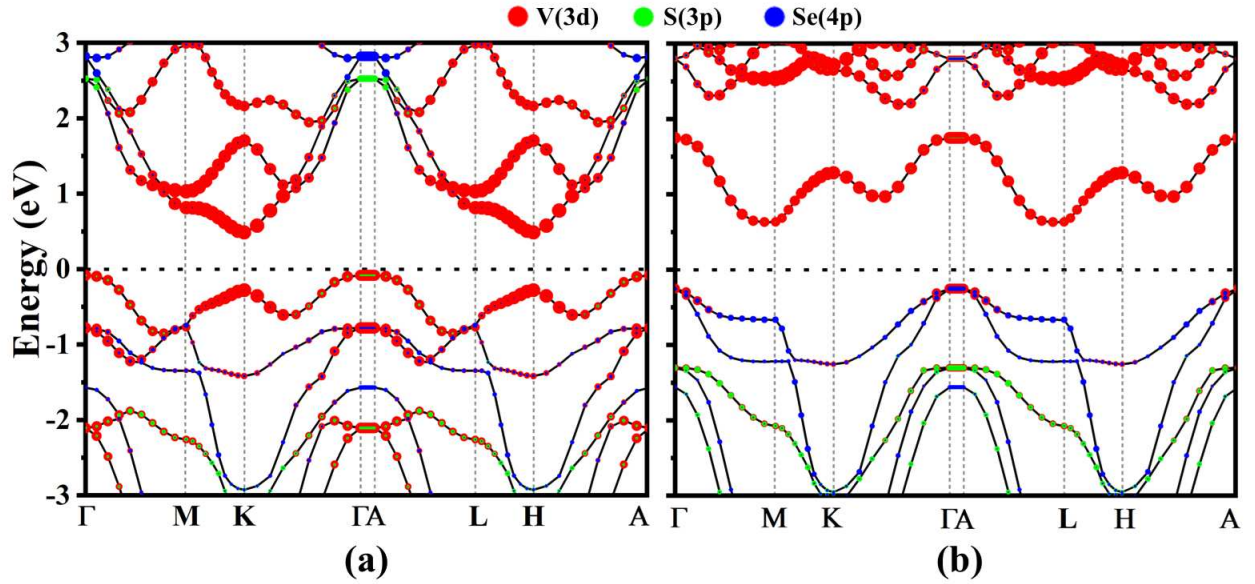


Figure S3. Projected band structures for (a) majority and (b) minority spin carriers of the Janus VSSe monolayer.

The broken horizontal mirror symmetry within the Janus VSSe monolayer gives rise to

spontaneous polarization normal to the plane, which is attributed to the inherent electric field ( $\mathbf{E}_{in}$ ). From the Bader charge analysis, we found that S and Se atoms gain 0.70e and 0.54e charges, respectively, from the V atom which loses 1.24e charge. It is clear that due to the electronegativity order: S (2.58) > Se (2.55) > V(1.63), S atom gains more electronic charge from V atom as compared to the Se atom, resulting in  $\mathbf{E}_{in}$  along the positive  $z$ -direction (upwards, i.e., from Se to S). The planar average of the electrostatic potential energy is taken along the  $z$ -direction as shown in Fig. S4. From Fig. S4, we can calculate the change in work function  $\Delta\Phi$  as we go from Se to S, and its value turns out to be nonzero (5 meV), further confirming the presence of  $\mathbf{E}_{in}$ .

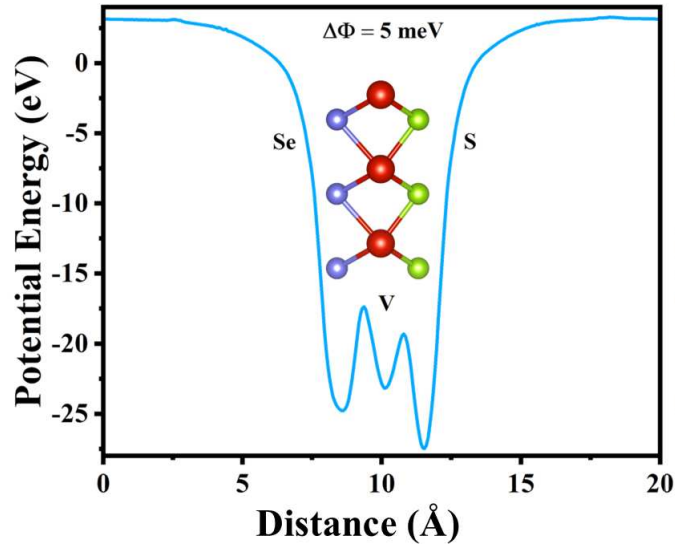


Figure S4. Planar average of the electrostatic potential energy as a function of distance along  $z$ -direction.

## B. Janus 2H-VSSe Bilayer

### 1. Different magnetic configurations and stability

Using 2x2 supercells of each of the considered stacking type, we have constructed seven different magnetic configurations which include an FM and six antiferromagnetic (AFM) configurations (see Fig. S5). The FM configuration possesses both interlayer and intralayer ferromagnetic coupling, with all the spins aligned in the same direction (Fig. S5(a)). The AFM1 configuration (Fig. S5(b)) is designed such that it is intralayer FM (spins within a

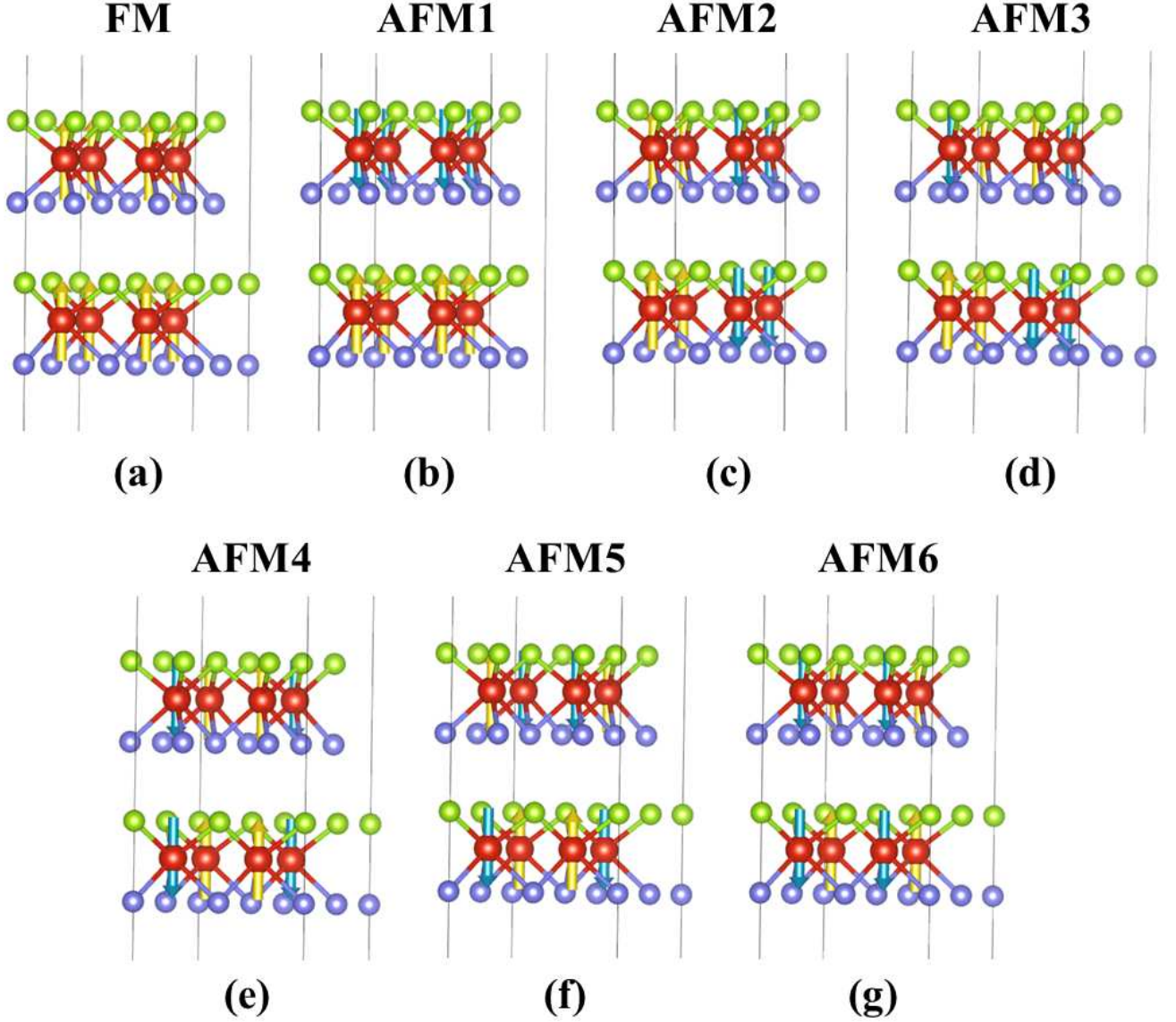


Figure S5. Different magnetic configurations considered for the AB stacked bilayer. Yellow and blue vertical arrows denote the majority and minority spins localized on Vanadium atoms, respectively. The same magnetic configurations were used for all the stacking arrangements considered in this work.

layer are aligned in the same direction) but interlayer AFM (spins of the two layers are equal and aligned opposite to each other). In the other considered AFM configurations, AFM2 - AFM6 (Fig. S5), the spins within each single layer are aligned opposite to each other and thus possess both inter- and intralayer AFM characteristics.



2. 3D Band Structure

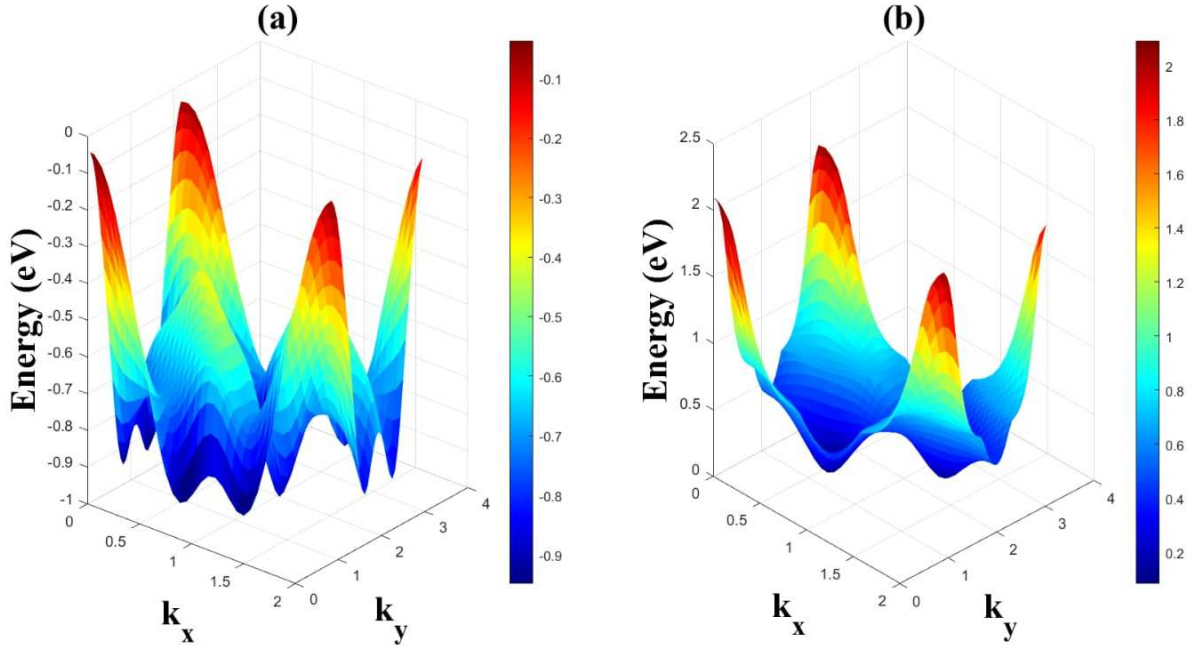


Figure S6. 3D plots of the (a) highest valence band and (b) lowest conduction band corresponding to the majority spin carriers at  $k_z = 0$  plane with  $E_F$  shifted to zero.

### 3. Effect of external electric field on the electronic properties

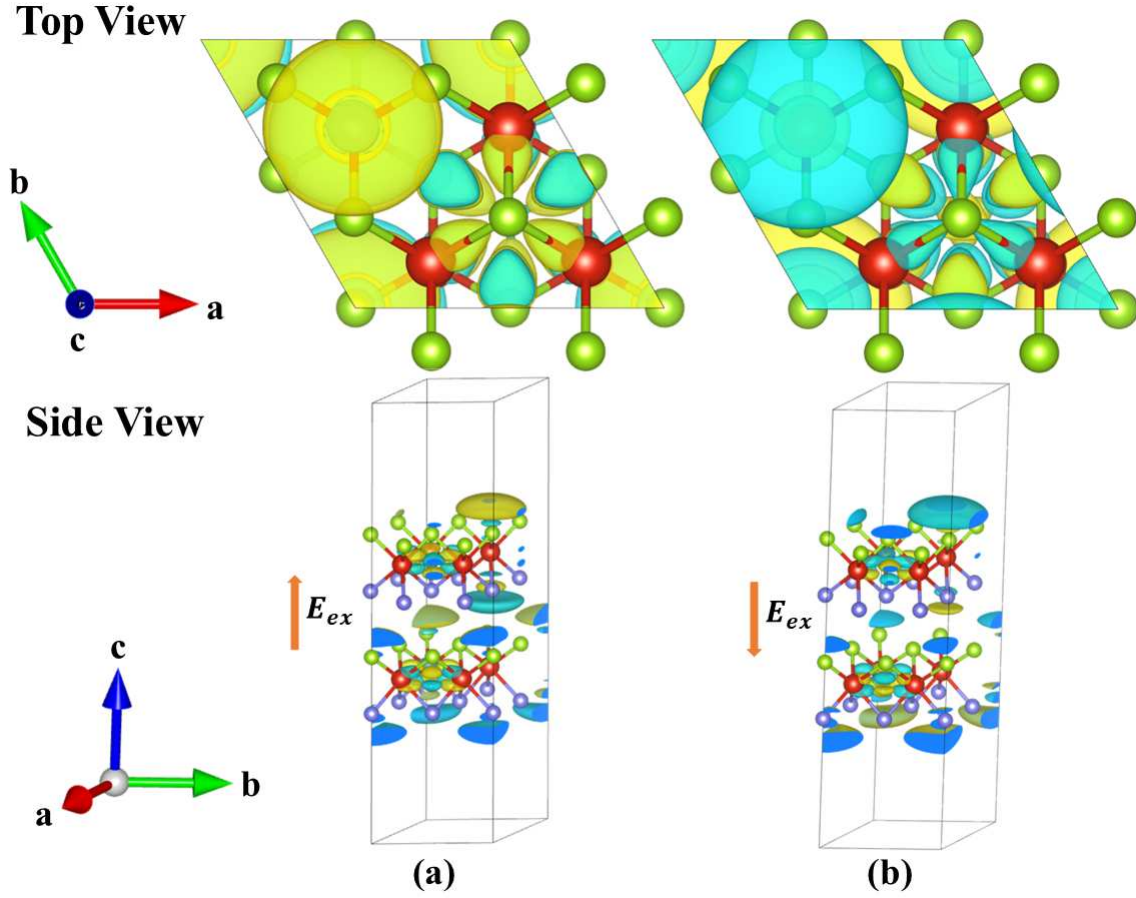


Figure S7. Charge density difference between the cases  $E_{ex} = 0.0$  and  $E_{ex} = 0.18 \text{ V/\AA}$  applied in the (a) upward and (b) downward directions of the considered VSSe bilayer. The yellow and blue colors correspond to the positive and negative isosurfaces at  $1.27 \times 10^{-4} \text{ e/\AA}^3$ , and depict the charge accumulation and depletion regions, respectively.

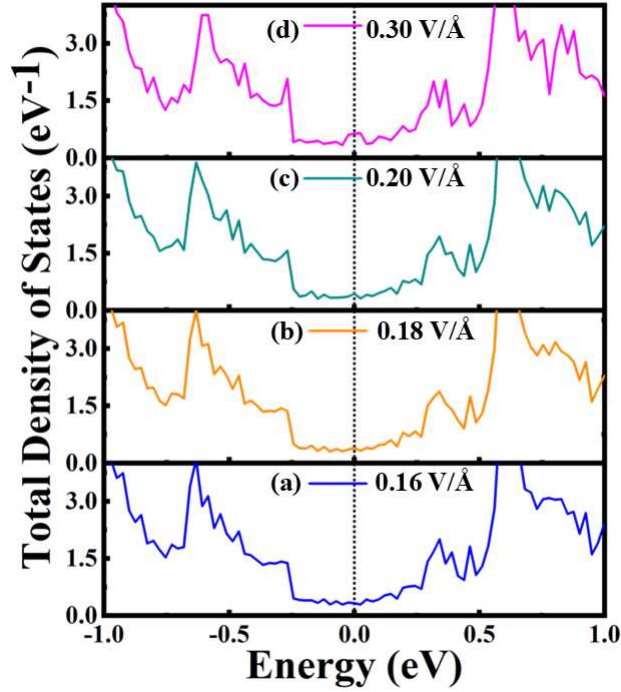


Figure S8. Total density of states (TDOS) of the majority spin carriers of the VSSe bilayer in the presence of external electric fields of intensities: (a) 0.16 V/Å, (b) 0.18 V/Å, (c) 0.20 V/Å, and (d) 0.30 V/Å, applied downward.

- 
- [1] Chunmei Zhang, Yihan Nie, Stefano Sanvito, and Aijun Du. First-Principles Prediction of a Room-Temperature Ferromagnetic Janus VSSe Monolayer with Piezoelectricity, Ferroelasticity, and Large Valley Polarization. *Nano Letters*, 19(2):1366–1370, Feb 2019.
  - [2] Dibyendu Dey and Antia S. Botana. Structural, electronic, and magnetic properties of vanadium-based Janus dichalcogenide monolayers: A first-principles study. *Phys. Rev. Mater.*, 4:074002, Jul 2020.
  - [3] Shengmei Qi, Jiawei Jiang, and Wenbo Mi. Tunable valley polarization, magnetic anisotropy and Dzyaloshinskii–Moriya interaction in two-dimensional intrinsic ferromagnetic Janus 2H-VSeX (X = S, Te) monolayers. *Phys. Chem. Chem. Phys.*, 22:23597–23608, 2020.
  - [4] Houlong L. Zhuang and Richard G. Hennig. Stability and magnetism of strongly correlated single-layer  $VS_2$ . *Phys. Rev. B*, 93:054429, Feb 2016.



- [5] A. H. M. Abdul Wasey, Soubhik Chakrabarty, and G. P. Das. Quantum size effects in layered  $VX_2$  ( $X = S, Se$ ) materials: Manifestation of metal to semimetal or semiconductor transition. *Journal of Applied Physics*, 117(6):064313, 02 2015.
- [6] Chaobo Luo, Xiangyang Peng, Jinfeng Qu, and Jianxin Zhong. Valley degree of freedom in ferromagnetic Janus monolayer H-VSSe and the asymmetry-based tuning of the valleytronic properties. *Phys. Rev. B*, 101:245416, Jun 2020.
- [7] Jing Zhang, Shuai Jia, Iskandar Kholmanov, Liang Dong, Dequan Er, Weibing Chen, Hua Guo, Zehua Jin, Vivek B. Shenoy, Li Shi, and Jun Lou. Janus Monolayer Transition-Metal Dichalcogenides. *ACS Nano*, 11(8):8192–8198, Aug 2017.
- [8] Jun Wang, Haibo Shu, Tianfeng Zhao, Pei Liang, Ning Wang, Dan Cao, and Xiaoshuang Chen. Intriguing electronic and optical properties of two-dimensional janus transition metal dichalcogenides. *Phys. Chem. Chem. Phys.*, 20:18571–18578, 2018.